Aquatic Biogeochemical Eddy Covariance Fluxes in the Presence of Waves

Matthew Herman Long[1]

[1]Woods Hole Oceanographic Institution

November 24, 2022

Abstract

The eddy covariance (EC) technique is a powerful tool for measuring atmospheric exchange rates that was recently adapted by biogeochemists to measure aquatic oxygen fluxes. A review of aquatic biogeochemical EC literature revealed that the majority of studies were conducted in shallow waters where waves were present, and that waves biased sensor and turbulence measurements. This review identified that larger measurement heights shifted turbulence to lower frequencies, producing a spectral gap between turbulence and wave frequencies. However, most studies sampled too close to the boundary to allow for a spectral turbulence-wave gap, and will require a paradigm shift in how EC measurements are conducted to remove wave-bias. EC fluxes have only been derived from the time-averaged product of vertical velocity and oxygen, often resulting in wave-biased fluxes. Presented here is a new analysis framework for removing wave-bias by accumulation of cross-power spectral densities below wave frequencies. This analysis framework also includes new measurement guidelines based on wave period, currents, and measurement heights. This framework is applied to sand, seagrass, and reef environments where traditional EC analysis resulted in wave-bias of 7.2 ± 5.8% error in biogeochemical (oxygen and H) fluxes, while more variable and higher error was evident in momentum fluxes (10.4 ± 20.5% error). It is anticipated that this framework will lead to significant changes in how EC measurements are conducted and evaluated, and help overcome the major limitations caused by wave-sensitive and slow-response sensors, potentially expanding new chemical tracer applications and more widespread use of the EC technique.

Aquatic Biogeochemical Eddy Covariance Fluxes in the Presence of Waves

Matthew H. Long[1]

[1]Marine Chemistry and Geochemistry Department, Woods Hole Oceanographic Institution, 266 Woods Hole Road, MS#8, Woods Hole, Massachusetts, USA, 02543

corresponding author: Matthew Long (mlong@whoi.edu)

Key Points:

- Literature review of eddy covariance studies reveals a majority of studies were conducted in shallow waters where waves bias measurements
- Sampling higher above the boundary shifts turbulence to longer scales, producing a spectral gap between wave and turbulent frequencies
- Paradigm shift in how studies are conducted and analyzed will enable the removal of wave bias and new chemical tracer applications

Abstract

The eddy covariance (EC) technique is a powerful tool for measuring atmospheric exchange rates that was recently adapted by biogeochemists to measure aquatic oxygen fluxes. A review of aquatic biogeochemical EC literature revealed that the majority of studies were conducted in shallow waters where waves were present, and that waves biased sensor and turbulence measurements. This review identified that larger measurement heights shifted turbulence to lower frequencies, producing a spectral gap between turbulence and wave frequencies. However, most studies sampled too close to the boundary to allow for a spectral turbulence-wave gap, and will require a paradigm shift in how EC measurements are conducted to remove wave-bias. EC fluxes have only been derived from the time-averaged product of vertical velocity and oxygen, often resulting in wave-biased fluxes. Presented here is a new analysis framework for removing wave-bias by accumulation of cross-power spectral densities below wave frequencies. This analysis framework also includes new measurement guidelines based on wave period, currents, and measurement heights. This framework is applied to sand, seagrass, and reef environments where traditional EC analysis resulted in wave-bias of 7.2 ± 5.8% error in biogeochemical (oxygen and H^+) fluxes, while more variable and higher error was evident in momentum fluxes (10.4 ± 20.5% error). It is anticipated that this framework will lead to significant changes in how EC measurements are conducted and evaluated, and help overcome the major limitations caused by wave-sensitive and slow-response sensors, potentially expanding new chemical tracer applications and more widespread use of the EC technique.

Plain Language Summary

The exchange of vital nutrients between the seafloor, overlying water, and the atmosphere is paramount to our understanding of the global cycling of these substances. Techniques that measure water transport and nutrients have revolutionized how these exchanges are studied, and how they impact local water quality, productivity, and nutrient cycling. Through measurements of the nutrient content of water, and their transport by water movement, the exchange of nutrients can be determined. These techniques were originally developed to examine exchange between the land and atmosphere, but applying these techniques to aquatic ecosystems has presented challenges due to surface waves that are present in the shallow aquatic ecosystems where these aquatic techniques are commonly applied. Waves cause errors in the sensors used to measure water transport and nutrients, and have presented significant challenges for applying these atmospheric techniques underwater. This research presents new guidelines for these aquatic exchange measurements that will require a paradigm shift in how measurements are conducted and analyzed, to allow for nutrient exchange measurements in the presence of waves. These new guidelines also allow for new sensors that were previously incompatible, expanding the applications of these techniques to new scientific research questions.

1 Introduction

Eddy covariance and related boundary layer exchange techniques have been used in terrestrial ecosystems since the early 1950s to measure fluxes of water and heat (Swinbank 1951) and are widely applied today to measure a variety of biogeochemical and energy fluxes in the atmospheric boundary layer (e.g. Baldocchi 2003, Lee et al. 2004, Burba and Anderson 2010). The physical oceanography community has applied this atmospheric boundary layer theory to fluxes of momentum, heat, and salt in marine settings, where waves have been identified as a unique source of bias in oceanic turbulence measurements (Trowbridge 1998, Scully et al. 2016, Trowbridge et al. 2018). The application of boundary layer theory to aquatic biogeochemical fluxes is comparatively new, and has mainly been used to examine oxygen (O_2) fluxes as a proxy for carbon exchange.

The aquatic eddy covariance (EC) technique measures the flux of solutes between the benthic surface and the overlying water (Berg et al. 2003, Lorrai et al. 2010, Reimers et al. 2012). EC measurements are widely considered the most reliable flux method because they require the fewest physical assumptions (Fairall et al. 2000). The aquatic EC technique has been used in challenging environments, where traditional methods are difficult to apply, such as benthic macrophytes (Hume et al. 2011, Koopmans et al. 2020), sea-ice (Long et al. 2012a, Glud et al. 2014), lakes (Brand et al. 2008, McGinnis et al. 2008), rocky substrates (Glud et al. 2010, Attard et al. 2019), oyster beds (Reidenbach et al 2013, Volaric et al. 2018), the deep sea (Berg et al. 2009, Donis et al. 2016), and coral reefs (Long et al. 2013; 2019, Rovelli et al. 2015) and represents a highly-advantageous methodology for examining high temporal resolution, ecosystem-level fluxes in complex environments. The aquatic EC technique has been occasionally applied to other tracers including temperature (Crusius et al. 2008, Long et al. 2012a, Else et al. 2015), salinity (Crusius et al. 2008), nitrate (Johnson et al. 2011), hydrogen sulfide (McGinnis et al. 2011) and pH (Long et al. 2015a). The aquatic EC technique has also been applied to the atmosphere-water interface to measure atmospheric O_2 exchange (Berg and Pace 2017; Long and Nicholson 2018) and at the oxycline and thermoclines in lakes (Kreling et al. 2014, Weck and Lorke 2017).

The basis for the EC technique is that turbulent mixing, caused by the interaction of current velocity with the benthic, atmospheric, sea-ice, or cline interfaces, is the dominant vertical transport process in boundary layers. Therefore, vertical fluxes across the ecosystem interfaces can be derived from high temporal resolution measurements of the vertical velocity and a solute concentration. The time-averaged EC flux across an interface are determined by:

$$Flux = \overline{w'c'} \qquad \textit{Eq. 1}$$

where the overbar represents a time average, and w' and c' are the fluctuating components of the vertical velocity and scalar concentration (c), respectively, that are measured at the same point at a fixed distance away from the interface.

Recent work has highlighted the influence of wave and current variability on EC measurements (Donis et al. 2015, Holtappels et al. 2015, Berg et al. 2015, Reimers et al. 2016a) when applying the most commonly used sensor in aquatic EC measurements, the Clark-type O_2 microsensor (Revsbech 1989). Studies demonstrating wave bias have indicated that automated numerical time-lag corrections (for slow or spatially separated sensors) can be biased by wave orbital motion (Berg et al. 2015, Donis et al. 2015), that cospectral analysis reveals significant contributions to fluxes at wave frequencies (Kuwae et al. 2006, Long et al. 2015b, Reimers et al. 2016a), and that Clark-type oxygen sensors can be biased by zero-crossing wave velocities

(Holtappels et al. 2015, Reimers et al. 2016a). These Clark-type microsensors have been designed to limit "stirring sensitivity" by reducing the tip size and microsensor design, but trade-offs exist between maximizing response time and reducing stirring sensitivity (Revsbech 1989). In comparison, optical O_2 sensors (i.e. optodes) have been applied more frequently since their introduction to aquatic EC (Chipman et al. 2012) because they have the advantage of not consuming O_2, making them less susceptible to stirring sensitivity as there is no net transport of O_2 to the sensor (Klimant et al. 1995). However, recent work has also suggested that optodes, like commonly used Clark-type sensors, may have a variable response time due to changes in the boundary layer thickness caused by wave motions or zero-crossing velocities that temporarily limit transport to the sensor, an effect that peaks at the frequency of the waves (Berg et al. 2015, Reimers et al. 2016a). To prevent sensor bias, microfluidic sensor housings (pumping fluid from the measurement point to negate wave velocities) and rotating instrument designs (preventing biased sensor separation corrections due to waves or orthogonal currents) have been developed, but also complicate instrument engineering (Long et al. 2015a, Long et al. 2019).

The issue of waves, which is unique to aquatic EC, has largely focused on the biogeochemical sensors, but wave bias in the turbulence measurements from acoustic sensors is also of major concern (Trowbridge 1998, Shaw and Trowbridge 2001, Scully et al. 2016). Wave-bias in the turbulent velocities used to calculate fluxes have been observed due to slight variations in instrument orientation, leading to some of the horizontal wave-associated velocities contaminating the vertical velocity (Trowbridge 1998, Long et al. 2015b, Reimers et al. 2016a, Scully et al. 2016, Trowbridge et al. 2018). This contamination of vertical velocity by waves is a problem when turbulence and surface waves are observed at similar or overlapping frequencies (Trowbridge 1998, Scully et al. 2016, Long and Nicholson 2018). However, a careful consideration of site hydrodynamic conditions and instrument configurations can enable a process to ensure the wave and turbulence frequencies do not overlap, thereby allowing for the spectral separation of turbulence and waves (Scully et al. 2016, Long and Nicholson 2018), effectively removing any effect that high-frequency surface waves have on chemical sensor or turbulence measurements.

Scully et al. (2016) describes and applies a procedure for removing wave bias in turbulence measurements in coastal settings, based on the frequency differences between turbulence and wave period (T_d). The Taylor frozen turbulence hypothesis relates wavenumber (k) to frequency (f) based on the mean advection speed (U), as:

$$k = \frac{2\pi f}{U} \qquad \textit{Eq. 2}$$

Both atmospheric and oceanic measurements of momentum cospectra suggest that under unstratified conditions, the peak of the variance preserving cospectra occurs at $k \sim 1/z$, where z is the height above the bottom where measurements are conducted (Wyngaard and Cote, 1972; Gerbi et al., 2008). Therefore, as long as the frequencies associated with the dominant surface waves ($1/T_d$) are high and the mean advection speed is low, all of the turbulent fluctuations will be at frequencies lower than the surface waves when:

$$\frac{2\pi z}{UT_d} > 1 \qquad \textit{Eq 3.}$$

For example, at common shallow water conditions where the values of T_d do not exceed 4 seconds and tidal currents are < 0.2 m s^{-1}, this relationship is easily satisfied if measurements are conducted at z = 0.4 m away from the benthic surface (i.e. [$(2\pi z)/(UT_d) = 3.1$]), whereas a measurement height at z = 0.1 m away from the benthic surface would not (i.e. [$(2\pi z)/(UT_d) = 0.8$]). This method has been used to calculate turbulent fluxes by filtering out frequencies at and above the wave frequencies and has demonstrated that there is typically a clear spectral gap between the frequency of the dominant surface waves and the dominant frequencies of the turbulent flux when measurements are conducted at sufficient heights away from the interface boundary (Scully et al. 2016).

This manuscript addresses a major issue that limits the application of boundary layer exchange techniques, specifically the aquatic eddy covariance technique, in shallow environments where waves are present. A primary objective of this highly interdisciplinary topic is to produce and communicate results that are easily discernable and translatable to the aquatic EC community. A review of existing aquatic EC literature is presented to highlight the predominance of EC applications in shallow water where waves are likely to be present, and the conditions and configurations of previous EC studies. A new analysis framework for flux calculation is presented, where the cross-power spectral density is accumulated from low frequencies, up to the wave frequencies, to calculate interface fluxes. This method effectively removes wave bias from both sensor and turbulence measurements, and specific guidelines are provided to ensure that this method can be applied, based on site hydrodynamics and instrument configurations. Also presented is the potential use of slow-response sensors using these same guidelines that will enable a wider range of sensors to be applied to the EC technique in the future.

2 Methods

2.1 Literature Review – This research presents a review of the EC literature consisting of 62 field-based manuscripts published since the introduction of aquatic oxygen EC for biogeochemical investigations (Berg et al. 2003). These manuscripts were separated to different study sites defined by either, having different measurement heights or, different water depths. In manuscripts where a range of sites with different depths were analyzed, the smallest and greatest depths are reported. The depths, measurement heights, solutes, sensors, benthic roughness elements, environment, burst length, and Reynolds decomposition method were extracted form manuscript text when reported. Cospectral frequencies and peak current velocities were taken directly from the text or visually estimated from figures. Measurement heights of the sensors were modified by subtracting biological canopy heights or physical barrier heights when reported.

2.2 Field Sites – The field sites were located ~7 km offshore of Key Largo, Florida, USA at the southern tip of Florida in the Florida Keys. The sites were located on or adjacent to Little Grecian Rocks Reef with a site on the reef crest (25.119016°N, -80.300504°W, Figure 1c) at 2.9 m mean depth, in a seagrass bed located ~225 m to the northwest of the reef site (25.120328°N, -80.302222°W, Figure 1b) at 4.8 m mean depth, and in a sandy site located ~300 m to the southwest of the reef site (25.117320°N, -80.303069°W, Figure 1a) at 6.3 m mean depth. The reef site is described in substantial detail (3-dimensional and species analyses) in Hopkinson et al. (2020), where the EC instrument can be seen near the center of the image analyses (in Figure 6 of Hopkinson et al. 2020) during its deployment in this study. This reef site is substantially degraded with its benthic surface and primary production dominated by octocorals, algae and rubble (Hopkinson et al. 2020, Owen et al. 2020). The seagrass site was dominated by dense *Thalassia testudinum* (turtlegrass) with a canopy height of 0.2 m underlain by carbonate sands. The sandy site was composed of carbonate sands with microalgal mats (Figure 1a) and migrating bedforms

0.1 m in height. Research was conducted from June 24 to June 29 in 2018 with the seagrass deployment beginning on the 24th and the sand and reef deployment beginning on the 25th of June, 2018.

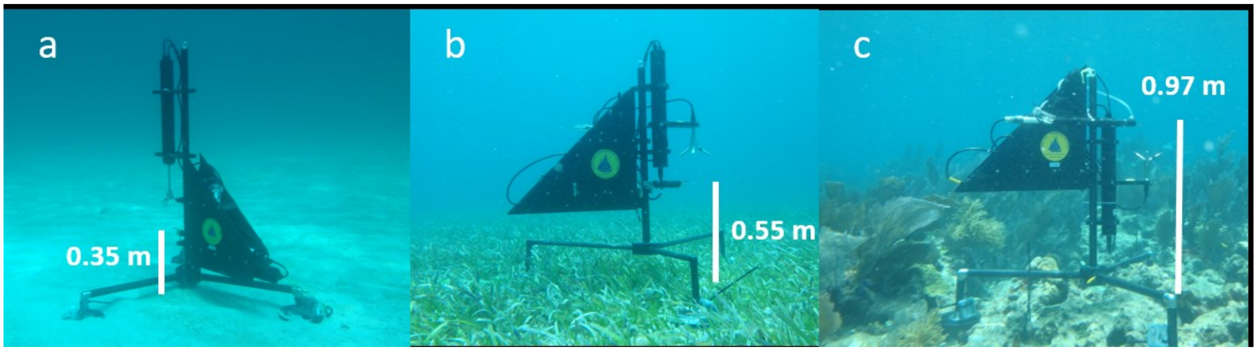

Figure 1. Eddy Covariance Hydrogen ion and Oxygen Exchange Systems (ECHOES) deployed at sand (a), seagrass (b) and reef (c) sites on or adjacent to Little Grecian Rocks Reef in the Florida Keys, Florida, USA. Measurement heights are indicated by white bars and text.

2.3 Instrumentation – The EC systems used here, known as Eddy Covariance Hydrogen Ion and Oxygen Exchanged System (ECHOES, Long et al. 2015a) consisted of an Acoustic Doppler Velocimeter (ADV, Nortek) that was coupled to a FirestingO_2 Mini fiber-optic O_2 meter with a fast-response (~ 0.3 s) 430 µm diameter optode (Pyroscience) (Long et al. 2015a, Long and Nicholson 2018, Long et al. 2019) and a fast-response (~0.6 s, Figure S1) Honeywell Durafet® III pH sensor with a preamp Cap Adapter and a custom isolation amplifier (based on Texas Instruments ISO124P). The ECHOES systems logged the three-dimensional velocity, depth, O_2 optode, pH sensor, and triaxial Inertial Measurement Unit (IMU, MicroStrain model 3DM-GX3) at a frequency of 16 Hz continuously. Using 6 rechargeable lithium ion batteries (50 Watt h, Nortek #220007) the system could operate continuously for ~4.5 days. All instrumentation was mounted to a light-weight, passively rotating carbon fiber frame (Figure 1). A bubble level affixed to the ADV mount allowed for precise leveling during field deployment by SCUBA divers. Stakes (sand and seagrass sites) or lead weights and zip ties (reef site) maintained instrument location and orientation. The measurement height, or location of the ADV measuring volume and sensors, above the sediment surface was determined by placing it at a height that was greater than twice the canopy or bedform height (Figure 1) as recommended by terrestrial EC guidelines where twice the canopy height, and up to 5 times the canopy height in patchy environments, is recommended (Burba and Anderson 2010, Long et al. 2015b).

The microfluidic flow-through sensor design has a small volume (0.33 cm^3) and a KNF Micropump (model NF10) with a flow rate (100 mL min^{-1}) that combine to have a quick flush rate (5 Hz) while protecting and preventing light interference for both O_2 and pH sensors. The microfluidic intake was located 0.025 m behind the ADV measuring volume (see Donis et al. 2015, Berg et al. 2015) to prevent disruption of ADV-measured flow rates (Long et al. 2015a). The microfluidic housing mounted tightly over the Durafet III sensor tip and has a small chamber for inserting the O_2 optode, that is located at the end of a 0.04 m long, 0.003 m inside diameter copper intake tube and filter, with the outlet of the microfluidic chamber connected to the pump intake (Figure S2). A passive flow meter (0-100 ml min^{-1}) connected to the pump outlet was used to confirm pumping rates during deployment.

A separate frame at each site contained an Odyssey (Dataflow Systems, New Zealand) photosynthetically active radiation (PAR) sensor and a Seabird SeapHOx (measuring salinity, temperature, depth, O_2, and pH). The SeapHOx was factory calibrated and the Odyssey PAR sensors were calibrated to a HR-4 spectroradiometer system (HOBI Labs HydroRAD-4) using the methods of Long et al. (2012b).

2.4 Eddy Covariance Analysis Framework – The 16 Hz data were averaged to 8 Hz for analysis. The ECHOES O_2 and pH sensors were calibrated to the slow-response SeapHOx sensors by least-squares regression. The pH was converted to H^+ ion concentration for all calculations. The ADV velocity data was removed from analysis when the beam correlation was < 50%. The means for Reynolds decomposition were determined using a 5 minute moving average window. The period over which the flux was determined, or burst length, was 15 minutes, with subsequent averaging to hourly rates. Rotations were conducted automatically by Nortek software (Vector v1.39.09) to East, North, and Up coordinates based on the IMU data (see Long and Nicholson 2018) followed by a planar rotation (see Lorke et al. 2013) for each instrument deployment. Standard eddy covariance analysis was conducted to calculate O_2 $\overline{(w'O_2{}')}$, H^+ $\overline{(w'H^{+\prime})}$, and momentum $\left(\overline{(w'u')^2} + \overline{(w'v')^2}\right)^{1/2}$ fluxes (e.g. Eq. 1) where u and v indicate the horizontal components of the velocity and w represents the vertical velocity. Cross Power Spectral Densities were also used to calculate O_2, H^+ and momentum fluxes and were determined with the Matlab function "CPSD", with the removal of wave frequencies conducted by accumulating the CPSD at frequencies below approximately $1/(2T_d)$. A storage correction was applied to all biogeochemical fluxes due to the presence of biological canopies and the high measurement heights used (Lorrai et al. 2010, Rheuban et al 2014a, Long and Nicholson 2018). Power spectral densities were determined using the Matlab function "PWELCH". The T_d was determined by finding the maximum of the momentum CPSD at the frequencies where the waves were expected for the study sites (e.g. 0.1 > Hz < 1). Wave velocities were estimated by:

$$wave\ velocity = \left(\overline{(u' - \overline{u})^2} + \overline{(v' - \overline{v})^2} + \overline{(w' - \overline{w})^2}\right)^{1/2} \qquad \text{Eq. 4}$$

where the prime indicates the instantaneous velocity and the overbars indicate averaging over each burst. Flux methods were compared by linear regression. The normalized root square error (NRSME) was determined by calculating the square root of the square of the difference between flux methods, averaging this value across each deployment and scalar, and normalizing this to percent by dividing by the range of the flux. This normalization method was used as the net, or average of the biogeochemical fluxes, is close to zero and would result in erroneous results.

3 Results

3.1 Literature Review - A total of 62 aquatic field-based biogeochemical EC manuscripts were identified (see Supplemental Information), which, when separated to individual studies based on different water depths and measurement heights, resulted in 102 studies for the purposes of this analysis (excluding this study). The use of Clark-type O_2 microsensors dominated (n = 80 studies, starting from Berg et al. 2003) with O_2 optodes becoming more popular recently (n = 20, starting from Chipman et al. 2012). Other sensors applied to EC included temperature (n = 5), galvanic O_2 (n = 2), conductivity (n = 1), nitrate (n = 1), hydrogen sulfide (n = 1), and pH (n = 1).

Previous studies have deployed the EC technique at water depths ranging from 0.3 to 2500 m, but the majority of these studies were conducted at depths of less than 5 m (n = 44, out of 80 studies reporting depth, Figure 2a). The mean peak current velocity of previous studies was 0.175 ± 0.219 m s^{-1}, with a median of 0.123 m s^{-1}, and a range of 0.015 to 1.8 m s^{-1} (Figure 2b). The mean measurement height of previous studies was 0.25 ± 0.17 m, with a median of 0.20 m, and a range of 0.04 to 0.80 m (Figure 2c). The majority of studies (n = 68, out of 99 studies reporting measurement heights) used measurement heights of less than 0.25 m above the bottom. Some studies reported physical or biological canopy roughness elements (n = 22), which were subtracted from the reported measurement heights, resulting in a corrected mean measurement height of 0.206 ± 0.178 m, a median of 0.15 m, and a range of -0.365 to 0.8 m.

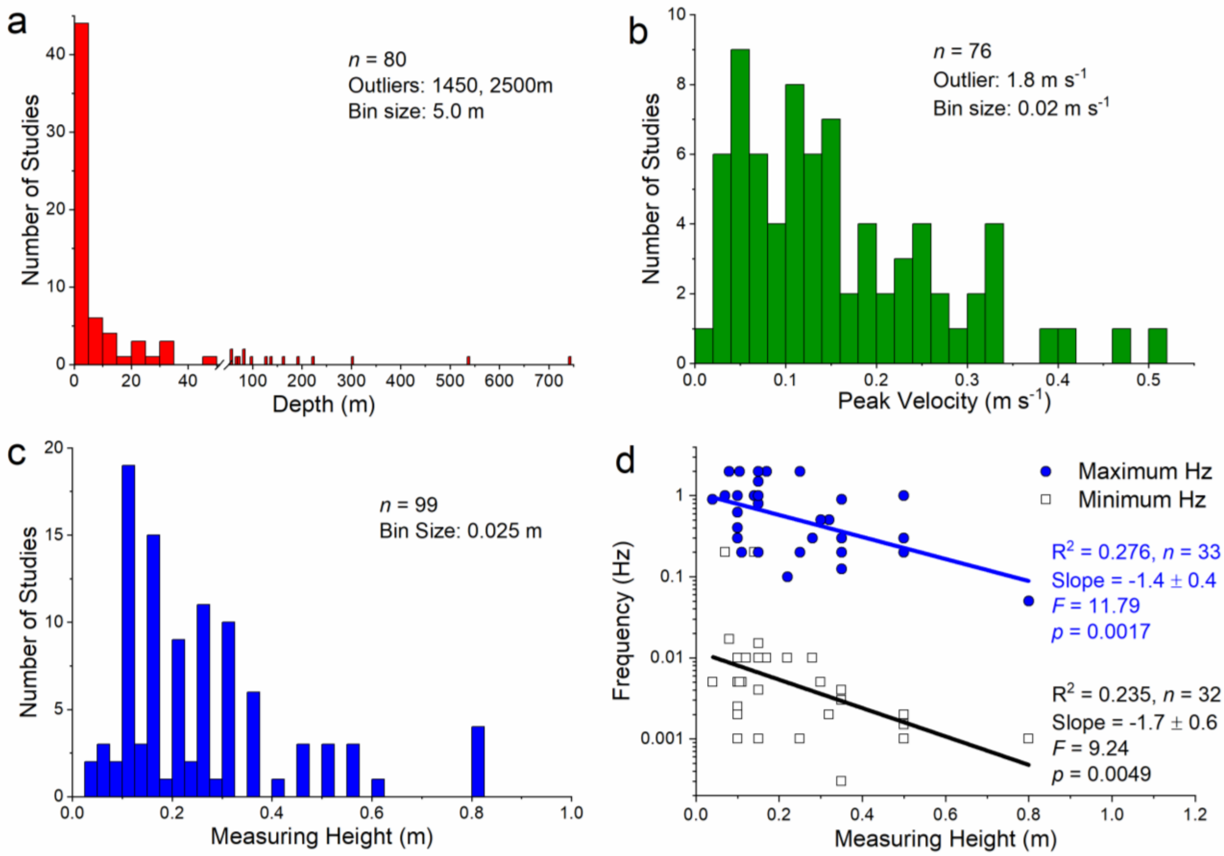

Figure 2. Histograms of the depth of biogeochemical eddy covariance studies (a) and the peak velocity measured in studies (b). Note the dominance of shallow-water studies where waves are likely present. Histograms of measurement heights (uncorrected for canopy or physical barrier heights) used in eddy covariance studies (c) and the associated frequencies of flux-carrying eddies which shift to longer scales with increasing measurement heights (d) where statistics represent a significant difference from a zero-slope line.

A total of 33 studies reported the contributing turbulent frequencies of the fluxes, which displayed a decrease in frequency with increased measurement height (Figure 2d). Both the highest and lowest contributing frequencies show a negative slope with increasing measurement height, and a significant difference from a zero-slope line. Applying Eq. 3 to all previous studies indicated that the mean of the conditions and instrument configurations may allow for the separation of turbulence and wave frequencies (Table 1). However, the majority of studies (n = 68) were conducted at measurement heights < 0.25 m and these low measurement heights combined with mean study conditions suggest that a distinct separation between turbulent and wave frequencies may not have been possible (Table 1).

Table 1. Demonstration of the potential for a spectral gap between turbulence and wave frequencies in different studies

Site	Mean Measurement Height (z) m	Peak Velocity (U) m s^{-1}	Wave Period (T_d) s	*Eq 3*: $(2\pi z/(UT_d)$
Previous studies (< 0.25m)	0.12 (-0.365 to 0.24 m, n = 68)	0.172	*4.0	1.08
All previous studies	0.21 (-0.365 to 0.8 m, n = 99)	0.175	*4.0	1.86
This study - Sand	0.35 (0.1m bedforms)	0.18	3.9	3.13
This Study - Grass	0.55 (0.2m canopy)	0.12	4.1	3.19
This Study - Reef	0.97 (0.5m canopy)	0.11	3.7	7.25

The * indicates assumed values as the majority of studies (n = 94) did not report wave period. When biological canopy or physical barrier heights are reported, these have been subtracted from the reported measuring heights (see Supplemental Information). Numbers in parenthesis are the range and n from previous studies, or canopy and beform heights (this study).

For conducting Reynolds decomposition, 33 manuscripts used linear detrending, 15 used a moving or running average window, 7 used a combination or other method, and 7 did not report a mean determination method. The burst length, or period over which fluxes are calculated, was most commonly 15 min (n = 43 manuscripts) followed by < 10 minutes (n = 5), 10 min (n = 4), 30 min (n = 3), 20 min (n = 1), variable (n = 1) or not reported (n = 5). A range of different data and time-series corrections including; velocity de-spiking (e.g. Goring and Nikora 2002), various coordinate rotations (Reimers et al. 2012, Lorke et al. 2013), sensor time-lag corrections (Donis et al. 2015, Berg et al. 2015), low frequency wave corrections (Reimers et al. 2016b), storage correction (Lorrai et al. 2010, Rheuban et al. 2014a. Long and Nicholson 2018), non-steady state condition bias (Holtappels et al. 2013), slow sensor response time correction (McGinnis et al. 2008), stirring sensitivity correction (Holtappels et al. 2015), and platform motion corrections (Long and Nicholson 2018) have been described and applied, and are discussed elsewhere, as noted.

3.2 Field Data – The three ECHOES and associated instruments were deployed for 4 - 4.5 days at each site (sand 96 h, seagrass 108 h, and reef 96 h; Figure 3) with a total of 84h of overlap where all 3 ECHOES were collecting data at the same time. In these relatively clear sub-tropical waters the ADV velocity beam correlation was used to remove time periods where the correlation was < 50 % which resulted in the removal of 35.4% (34 h), 0.1% (0.75 h), and 2.3% (4.25 h) of the data from the sand, seagrass, and reef sites, respectively (Table 2). At the reef site a substantial amount of pH data was lost due to sporadic electrical issues that contaminated 72.4% (69.5 h) of the data. Fluxes showed expected diel trends with O_2 production and H^+ consumption during the day and O_2 consumption and H^+ production during the night (Figure 3a-f). Biogeochemical fluxes were about an order of magnitude larger on the reef site compared to the sand site. Current velocities were dominated by diurnal tides and wave velocities generally decreased over the deployment period (Figure 3d-i). Diel ranges of O_2 (171 to 237 µmol L^{-1}) and pH (8.06 to 8.17) were very similar between the adjacent sites.

Table 2. Comparison of direct covariance, CPSD(All Hz), and CPSD (<0.125 Hz) fluxes

			Covariance vs. CPSD (All Hz)			Covariance vs. CPSD (<0.125 Hz)		
Flux	Site	n	Slope (±SE)	R^2	NRSME	Slope (±SE)	R^2	NRSME
Oxygen	Sand	248	1.02 ± 0.01	0.996	1.0 ± 0.9 %	0.91 ± 0.01	0.946	2.7 ± 5.5 %
	Seagrass	429	1.03 ± 0.00	0.997	0.8 ± 0.6 %	0.89 ± 0.02	0.883	2.9 ± 8.0 %
	Reef	375	1.02 ± 0.01	0.993	0.7 ± 0.7 %	0.57 ± 0.03	0.543	4.1 ± 10.2 %
	Total	1052	1.02 ± 0.00	0.994	0.3 ± 0.9 %	0.66 ± 0.02	0.644	1.7 ± 10.8 %
H^+	Sand	248	1.03 ± 0.01	0.957	2.5 ± 1.8 %	0.62 ± 0.03	0.590	7.2 ± 5.8 %
	Seagrass	429	1.03 ± 0.00	0.998	0.5 ± 0.5 %	0.93 ± 0.01	0.970	1.3 ± 2.1 %
	Reef	106	1.03 ± 0.03	0.920	1.4 ± 7.1 %	0.87 ± 0.05	0.738	3.1 ± 9.1 %
	Total	783	1.03 ± 0.01	0.945	0.2 ± 5.6 %	0.88 ± 0.02	0.788	0.5 ± 8.2 %
Momentum	Sand	248	1.00 ± 0.00	0.999	0.2 ± 0.6 %	0.03 ± 0.00	0.479	5.0 ± 21.5 %
	Seagrass	429	1.00 ± 0.00	0.999	0.2 ± 0.6 %	0.00 ± 0.01	0.001	5.7 ± 24.0 %
	Reef	375	1.01 ± 0.00	0.999	0.2 ± 0.6 %	0.03 ± 0.00	0.542	10.4 ± 20.5 %
	Total	1052	1.01 ± 0.00	0.999	0.1 ± 0.6 %	0.04 ± 0.00	0.523	4.3 ± 22.9 %

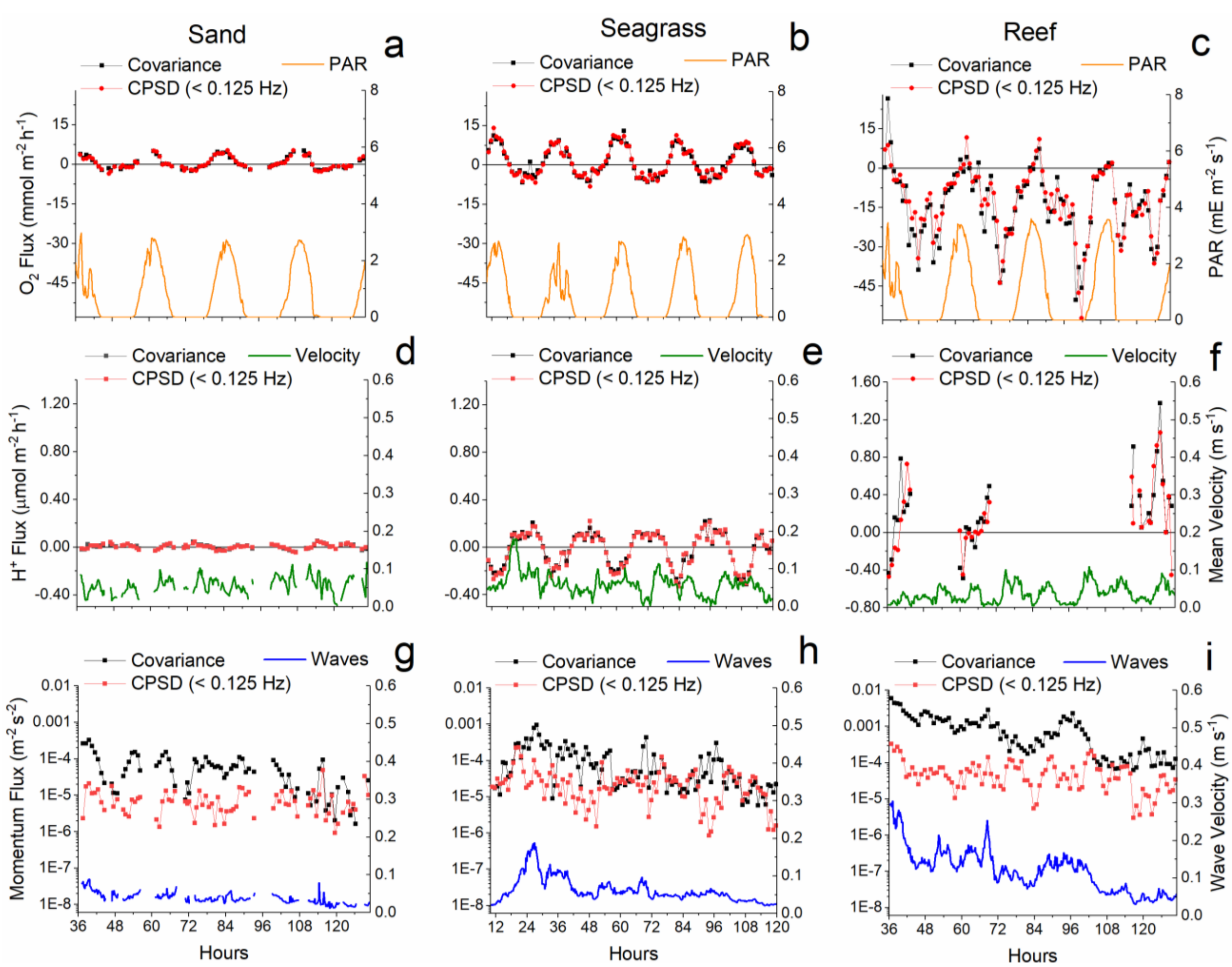

Figure 3. Time series data and fluxes at sand, grass, and reef sites beginning at noon (hour 12) on June 24, 2018. Oxygen (left a, b, c), H^+ (left d, e, f) and momentum (left g, h, i) fluxes determined

by eddy covariance (black) and cross-power spectral densities accumulated below wave frequencies (< 0.125 Hz, red). Time series of photosynthetically active radiation (PAR, orange; a, b, c), mean velocities (green; d, e, f) and wave velocities (blue; g, h, i) are shown on the right axes.

Applying Eq. 3 to the study conditions suggests that there was a spectral gap between wave and turbulent frequencies (i.e. Eq. 3 > 3.1, Table 1). Before applying this theory, the agreement between fluxes calculated using traditional direct covariance analysis (e.g. Eq. 1) was compared to that of the Matlab CPSD function, accumulated across all frequencies. Across the sites (sand, grass, and reef) and scalars (O_2, H^+, momentum) the minimum R^2 was 0.92 with a maximum of 2.5 % normalized root square mean error (NRSME, Table 2, Figure 4). These lowest values were found for the scalar with the least data (n = 108 bursts, Reef H^+, Table 2) and the site with the least data and smallest fluxes (n = 248 bursts, Sand H^+, Table 2, Figure 3d), respectively. The remaining majority of results had coefficients of determination of ≥ 0.99 and ≤ 1.0 % error (Table 2) indicating good agreement between direct covariance and CPSD methods (Figure 4).

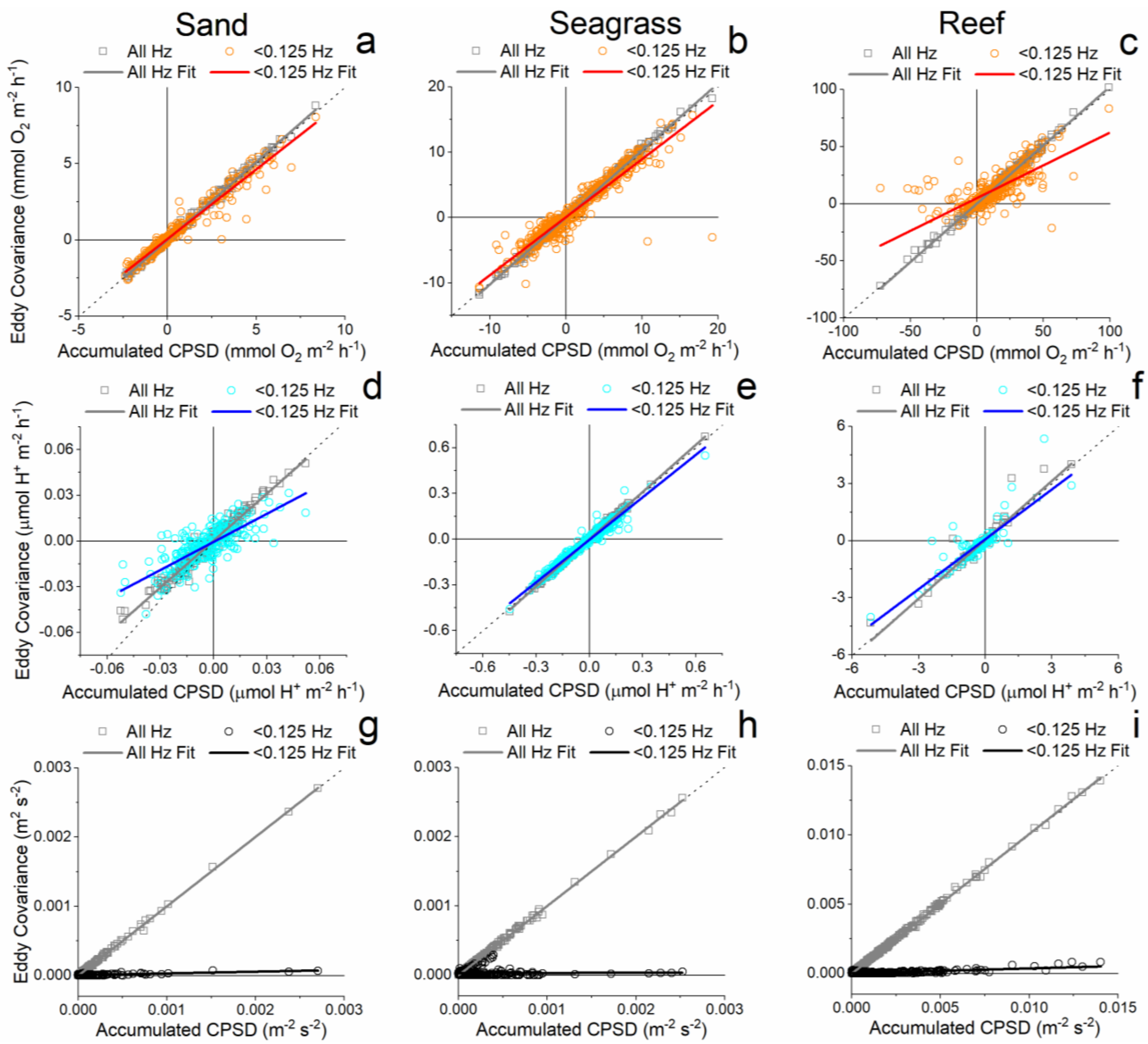

Figure 4. Comparison of fluxes determined from the cross-power spectral densities, accumulated across all frequencies, and fluxes determined from eddy covariance (grey boxes, grey lines, a-i)

for the sand, grass, and reef sites. The comparison of fluxes determined from cross-power spectral densities, accumulated up to the wave frequency (< 0.125 Hz), and fluxes determined from eddy covariance are shown for O_2 (orange circles and red lines, a-c), H^+ (cyan circles and blue lines, d-f), and momentum (black circles and black lines, g-i) fluxes. Each symbol represents an individual 15 min burst and all lines are linear regressions with statistics reported in Table 2.

The wave period (T_d) at the sand, grass, and reef sites were 4.0 ± 0.5 (3.1 to 5.7 range), 3.9 ± 0.5 (2.6-5.2 range) and 3.7 ± 0.6 (2.0-5.3 range) s, respectively. By examining the power spectral density of the horizontal velocity (e.g. Figure 5d-f, Figure 6 d-f), especially during periods of high wave velocity and long wave periods, a cutoff frequency (F_c) of 0.125 Hz (8 seconds) was chosen as the frequency up to which the CPSD should be accumulated to remove wave bias (Figure 5, 6). In all cases (scalars and sites) the coefficients of determination and slopes were reduced and the error increased indicating that the frequencies associated with the waves were contributing to the flux (Table 2). The maximum decrease in the slopes (44%) and error (7.2 ± 5.8 %) was modest for the O_2 and H^+ fluxes compared to the substantial decrease in the slope (99%) and increase in error and variance (10.4 ± 20.5) for the momentum fluxes (Table 2, Figure 4). During periods of low wave activity, the accumulated CPSD commonly reached a distinct peak or plateau before the F_c under low wave conditions and had little impact on biogeochemical fluxes (Figure 5a-c). In the majority of cases, the momentum flux exhibited significant bias at wave frequencies (Figure 4h-j, Figure 5a-c, Figure 6 a-c). During conditions when the wave velocities were at least twice as high as the mean flow (occurring 7.3 %, 12.3 % and 66.5 % of the time at the sand, grass and reef sites, respectively) there was substantial contributions to all of the fluxes at wave frequencies (i.e. Figure 6 a-c). This was most evident during extreme conditions at the reef site, where the wave velocities were an order of magnitude greater than the current velocity (Figure 6c). The wave velocities were 10-fold greater than the mean velocity 18.1 % of the time at the reef site but were never 10-fold greater than the mean velocity at the sand and grass sites. Oxygen and H^+ power spectra (Figure 5, 6) showed no variability at wave frequencies while horizontal and vertical velocity spectra indicated a significant power at wave frequencies (Figure 5, 6). Further, differences between sites and sampling heights (i.e. sand, 0.35 m sampling height, Figure 5d, 6d) indicated substantial power at wave frequencies predominantly in the horizontal spectra, where wave orbitals become compressed vertically when sampling closer to the bottom, while the reef (0.97 m sampling height) indicate a balance between power at wave frequencies in both the horizontal and vertical (Figure 5f, 6f). Across the sites, the absolute differences between the hourly eddy covariance and CPSD fluxes (i.e. Figure 3a-c) were positively correlated to the wave velocity with slopes significantly different from zero and the strongest coefficient of determination for the momentum flux (R^2 = 0.71) followed by the O_2 flux (R^2 = 0.32), and H^+ flux (R^2 = 0.06) (Figure S3).

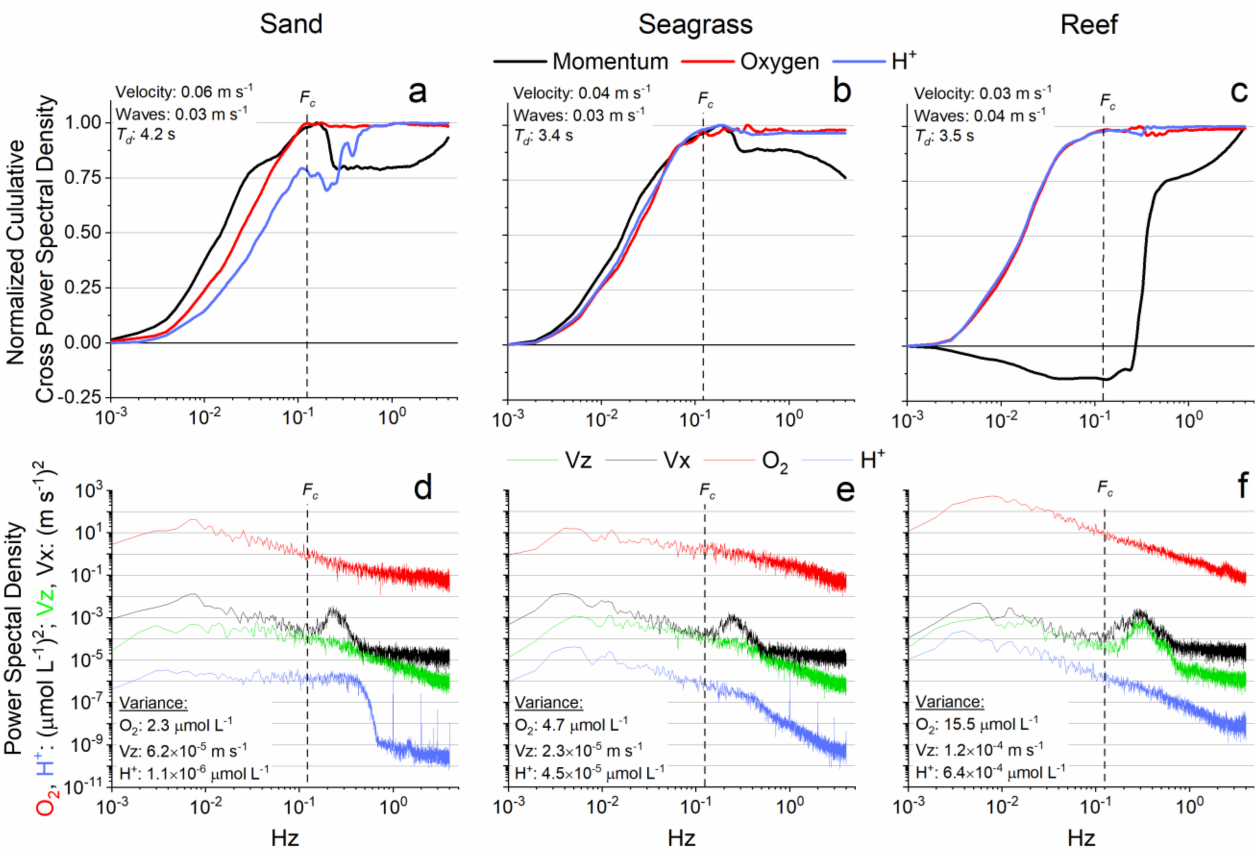

Figure 5: Spectral data from a low wave-energy period (hour 116, Figure 3). Normalized cumulative cross-power spectral densities show distinct differences between momentum fluxes and biogeochemical fluxes at wave frequencies. Oxygen and H^+ spectra (lower panels, red and blue, respectively) show no variability at wave frequencies while horizontal (Vx, black) and vertical velocity (Vz, green) spectra indicate a significant power at wave frequencies. Further, differences between sites and sampling heights (i.e. sand, 35cm sampling height) indicate substantial power at wave frequencies in the horizontal spectra, where wave orbitals become compressed vertically when sampling closer to the bottom, while the reef (lower right, 97cm sampling height) indicate a balance between power at wave frequencies in both the horizontal and vertical. Mean current velocities, wave velocities, and wave period are shown in text where wave and current velocities were of the same order of magnitude (a-c). The variance of oxygen, vertical velocity, and H^+ (text, d-f) over each period indicate an increase in both biogeochemical tracer and vertical turbulence variances from the sand to reef sites.

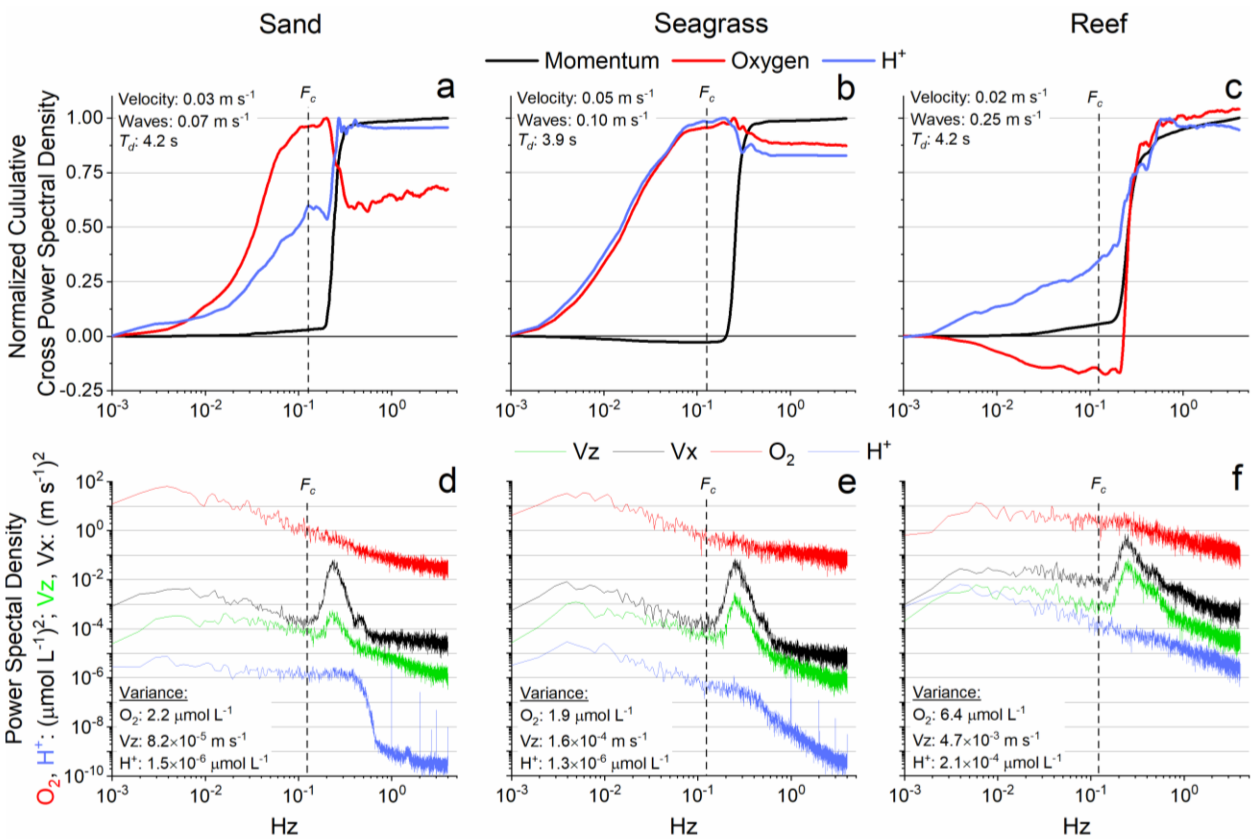

Figure 6: Spectral data from a high wave-energy period (hour 38, Figure 3). Cumulative cospectral densities show distinct differences between momentum fluxes and biogeochemical fluxes. Oxygen and H^+ spectra (lower panels, red and blue, respectively) show no variability at wave frequencies while horizontal (Vx, black) and vertical velocity (Vz, green) spectra indicate a significant bias by waves. Further, differences between sites and sampling heights (i.e. sand, 35cm sampling height) indicate substantial power at wave frequencies in the horizontal spectra, where wave orbitals become compressed vertically when sampling closer to the bottom, while the reef (lower right, 97cm sampling height) indicate a balance between power at wave frequencies in both the horizontal and vertical and potential bias in the cospectra of the biogeochemical fluxes (a-c). Mean current velocities, wave velocities, and wave period are shown in text where wave velocities were twice as large as the current velocities at the sand and grass sites (a-b) and an order of magnitude larger at the reef site (c). The variance of oxygen, vertical velocity, and H^+ (text, d-f) over each period indicate an increase in both biogeochemical tracer and vertical turbulence variances from the sand to reef sites.

3.3 Ecosystem Fluxes - The hourly O_2 and H^+ CPSD (<0.125 Hz) fluxes across each deployment (Figure 3a-f) were averaged by hour of day (Figure 7a, c) to enable the calculation of net daily fluxes averaged over the ~4 day deployments (Figure 7b, d). The method of calculation of net ecosystem metabolic (NEM) rates (e.g. Rheuban et al. 2014a) was chosen due to the significant data gaps in the sand O_2 and H^+ and reef H^+ fluxes (Figure 3). Both sand and seagrass sites exhibited net positive O_2 fluxes and autotrophy (11.8 ± 4.1 and 23.8 ± 9.2 mmol O_2 m^{-2} d^{-1}, respectively) while the reef site had net negative O_2 fluxes and strong heterotrophy (-304.8 ± 40.9 mmol O_2 m^{-2} d^{-1}) (Figure 7b). The seagrass site had net negative H^+ fluxes indicating a consumption of acidity (-0.39 ± 0.26 µmol H^+ m^{-2} d^{-1}), the sand site had near-balanced H^+ fluxes indicating no significant net production or consumption of acidity (0.07 ± 0.06 µmol H^+ m^{-2} d^{-1}), and the reef site had net positive H^+ fluxes indicating significant net acidity production (4.61 ± 1.30 µmol H^+ m^{-2} d^{-1}) (Figure 7d).

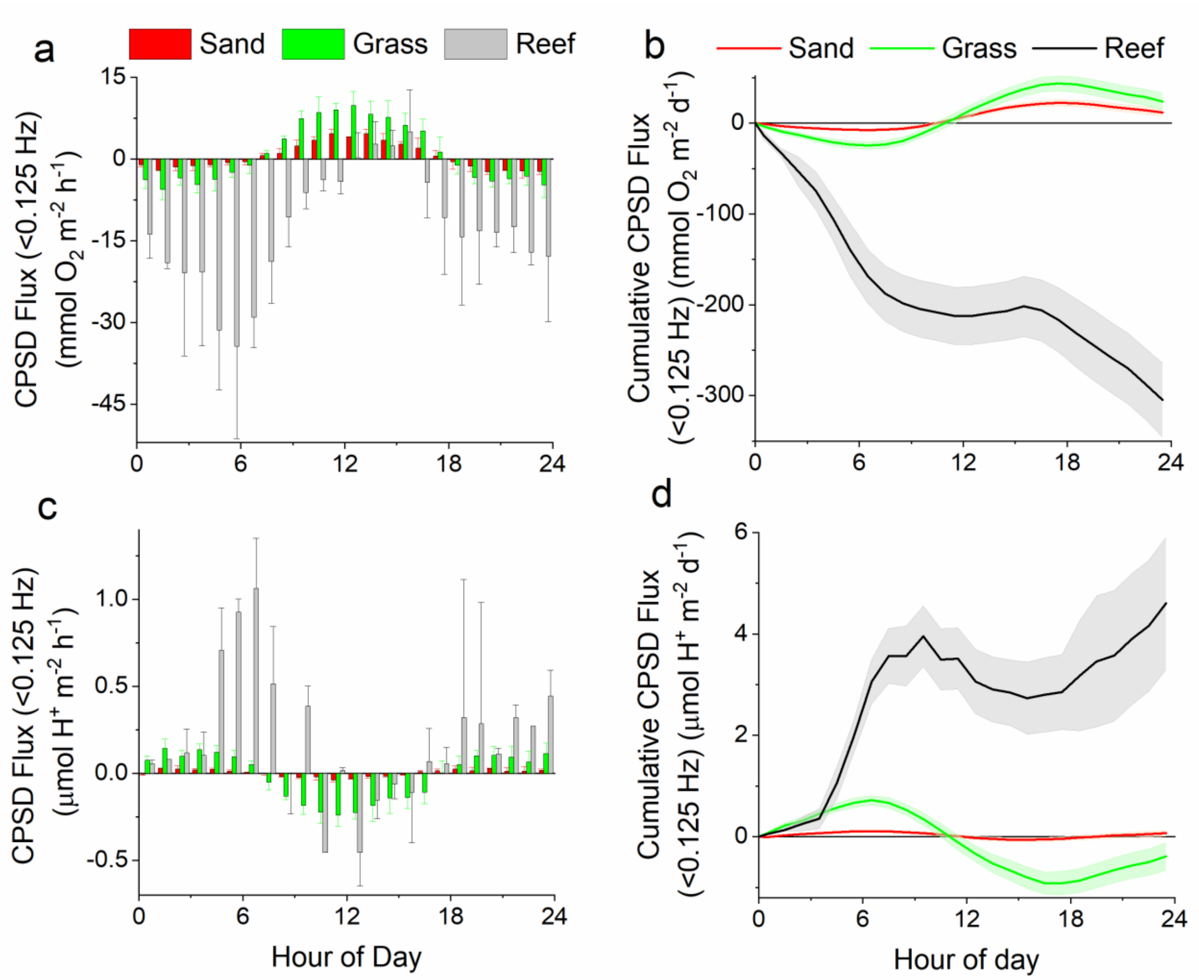

Figure 7. Accumulated cross power spectral density (<0.125 Hz) O_2 (a) and H^+ (c) fluxes averaged by hour of day from all data in Figure 3a-f for sand (red), seagrass (green) and reef (grey) sites. The fluxes were accumulated across the hour of day, where shading indicates propagated error, to produce a net daily O_2 (b) and H^+ (d) fluxes for each site.

4 Discussion

This research presents a new analysis framework and measurement requirements to enable biogeochemical EC measurements in the presence of waves. Since most studies using the EC technique have been conducted in shallow waters where waves are common, this has represented a significant setback for the small, but rapidly expanding biogeochemical EC community. Essentially, by measuring higher above the boundary than has been done traditionally (mostly < 0.25 m), the turbulent frequencies shift to longer scales, above the wave frequencies. The presented spectral analyses framework has been used to calculate turbulent fluxes by filtering out wave frequencies and has demonstrated that there is a clear spectral gap between the frequency of the dominant surface waves and the dominant frequencies of the turbulent flux when measurements are conducted at sufficient distance away from the interface (Scully et al. 2016). Here, spectral analysis reveals conditions and measurement heights that produce gaps between turbulence and wave frequencies in both scalar (e.g. O_2 and H^+) and turbulence measurements. Therefore, waves can be spectrally filtered and effectively remove bias in both chemical sensor and turbulence measurements, which also allows for new EC chemical sensors that have slower response times to be applied to the EC technique.

4.1 Literature review – The review of field-based biogeochemical EC studies revealed that the majority of studies have been conducted in shallow environments where waves are likely to occur. This potential for wave bias is compounded by the fact that the majority of studies (78%) used Clark-type microsensors, that have known biases created by wave-associated velocities and frequencies (Donis et al. 2015, Holtappels et al. 2015, Berg et al. 2015, Reimers et al. 2016a). The majority of studies sampled < 0.25 m from the bottom boundary (69%, 0.12 m mean when corrected for roughness elements) and it is likely that many of these studies would not exhibit a clear separation between wave and turbulence frequencies, as described in Eq. 3, which is illustrated by the color-mapped surface in Figure 8a. However, it is apparent that some previous studies could benefit from the presented spectral analysis framework, and that using higher measurement heights will benefit future studies (e.g. Figure 8b).

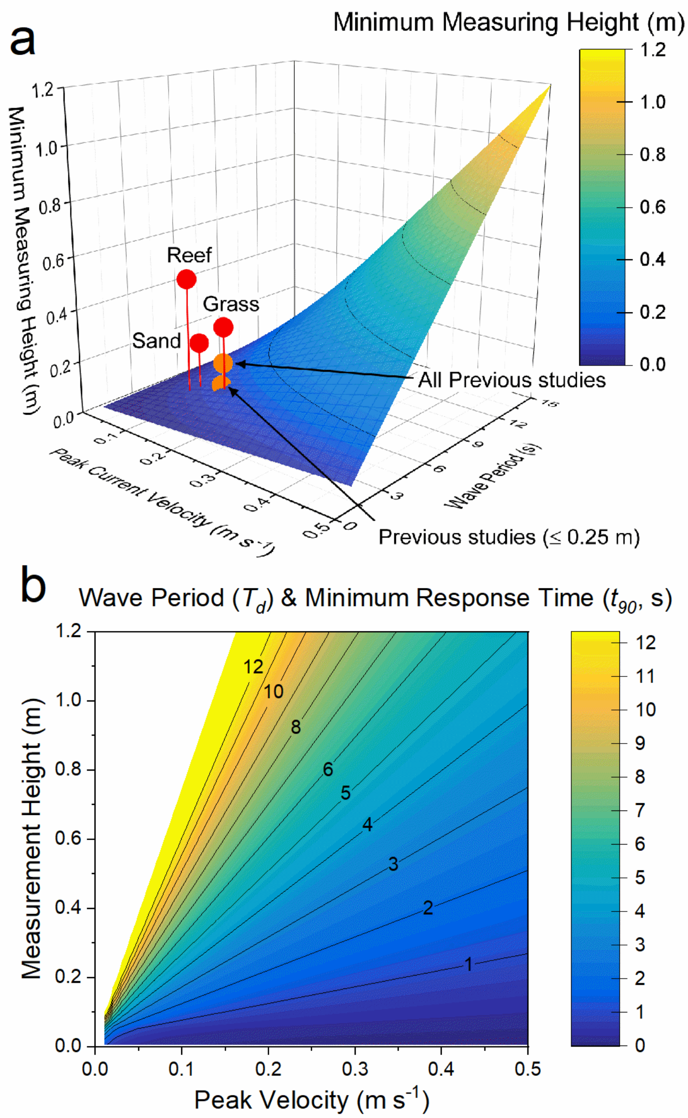

Figure 8: Minimum sampling heights that allow for a distinct gap between turbulence and waves frequencies based on $(2\pi z)/(UT_d)$ =1 (Eq. 3, Scully et al. 2016) (a). Individual points show sampling heights over sand, grass, and reef sites in this study minus the characteristic roughness heights of 0.1 (bedforms), 0.2 (seagrass canopy), and 0.5 m (reef canopy), respectively (red dots, Table 1). The Mean of Previous Studies represents the average measurement heights and peak current velocities (and an assumed T_d of 4 s) from the all previous studies and those conducted with a measurement height of < 0.25 m in Figure 1 (orange dots, Table 1). Rearranging the equation $(2\pi z)/(UT_d)$ =3.1 (the minimum value demonstrated in this study to allow for separation of turbulence and wave frequencies) to solve for T_d and color shading by the assumption that the minimum response time is approximately the T_d (or the Nyquist frequency (2x) of the cutoff frequency [$F_c \approx 1/(2T_d)$]), produces a recommended minimum response time (t_{90}, b) based on site conditions.

4.2 CPSD analyses framework – The presented CPSD analysis framework begins with a careful consideration of the site conditions, which inform appropriate measurement heights to allow for the spectral separation of turbulence and waves. When data is collected at appropriate measurement heights, the data can then be analyzed in the frequency domain, where the CPSD can be used to determine fluxes and wave periods can be evaluated. This spectral analyses can then be used to remove wave frequencies, by accumulating the CPSD up to the wave frequencies, effectively removing sensor and turbulence wave biases. Accumulating the CPSD across all frequencies can be used to compare with standard eddy covariance analyses, as well as determining the contribution to fluxes at wave frequencies. While this method is mostly applicable to sites with high frequency surface waves and moderate current velocities, it is noted that these are the predominate conditions for most biogeochemical eddy covariance studies to date.

The presented CPSD method, when accumulated across all frequencies, showed a very good agreement with traditional eddy covariance analysis with slopes of 1.0, $R^2 \geq 0.92$, and error $\leq 2.5\%$, where the lowest R^2 and highest error were found for H^+ fluxes with the least data and smallest fluxes, respectively. When the CPSD was accumulated only up to the wave frequencies (i.e. the cutoff frequency, F_c) there was a decrease in the flux in all cases, with a substantial decrease in the momentum flux, followed by less pronounced decreases for the biogeochemical tracers of O_2 and H^+. The large decrease in the momentum flux is expected as waves bias both horizontal and vertical velocities that are used to calculated the momentum flux, while O_2 and H^+ sensors are not affected at wave frequencies as they are located in a microfluidic housing that removes wave velocities by placing the sensors in a constant-flow environment. However, wave bias is still present during high-wave periods due to the vertical velocities used to calculate the biogeochemical fluxes, albeit much lower than the momentum fluxes that includes both horizontal and vertical wave components.

The fluxes generally reached a maxima or plateau before reaching the F_c, demonstrating the relationship in Eq. 3, where there is a distinct spectral gap between the turbulence and wave frequencies. During extreme wave conditions at the reef site, where current velocity was 10-fold lower than wave velocities, this was not always apparent (e.g. Figure 6c), but this is likely due to the limited cross-power spectral density at these low current velocities (i.e. the relatively flat velocity spectra at turbulence frequencies, <0.125 Hz), as opposed to wave bias, as the spectra clearly show the wave frequencies well above the F_c. Further, if wave and turbulent frequencies overlap during some study periods, for example during periods of low wave frequency (or high T_d) and high current velocity, it is straightforward to exclude these data from analysis based on Eq. 3.

In a previous study by this author, Long et al. (2015c), the presented cumulative cospectrum (Figure 8f in Long et al 2015c) illustrate an ideal application of the presented CPSD methodology, as there is a distinct separation between the turbulence and wave frequencies. In this example the measurement height was 0.175 m (0.35 m measurement height - 0.175 m seagrass canopy height), flow velocities were very low (0.011 m s^{-1}) and wave periods were very fast (~1.4 s) (Long et al. 2015c). Applying these parameters to Eq. 3 results in a value of 71.4, suggesting a substantial gap between turbulence and wave frequencies, which is apparent in the cumulative cospectrum that indicate a flux plateau and stable maximum from 0.1 Hz up to the wave frequencies (~0.5 to 1 Hz). In another EC study, by Kuwae et al. (2006), where current velocities from ~ 0.1 to 0.2 m s^{-1}, wave periods of 1-4 seconds, and measurement heights of 0.07 to 0.17 m produced values of Eq 3. of 0.6 to 10.7, suggesting that the CPSD method could also be applied to their study site. Kuwae et al. (2006) shows cumulative spectra and cospectra that 1.) illustrate wave-biased vertical velocity spectrum with no effect in O_2 spectrum, 2.) a typical turbulence-dominated cumulative cospectrum with frequencies from 0.01 to a stable maxima at 0.2 Hz and a negative contribution at 1-2 Hz, and 3.) cumulative cospectra that indicate significant contributions at wave frequencies from 0.2 to 1 Hz. These examples from Kuwae et al. (2006) are similar to the full-frequency spectra and cospectra presented in this study, notably for 1.) Figure 5, 6 e-f, 2.) Figure 6a-c, and 3.) Figure 6c. These previous studies were conducted with Clark-type microsensors which have been shown to be biased by wave orbital velocities (Berg et al. 2015, Donis et al. 2015, Holtappels et al. 2015, Reimers et al. 2016a) but these previous studies also suggest that wave velocities may cause scalar transport through the advection of porewater (Kuwae et al. 2006) or advection of tubulent motions or scalar variances through a fixed measurement point (Lumley and Terray 1983, Gerbi et al. 2008, Long et al. 2015c, Long and Nicholson 2018). Whether these wave-frequency variations are due to sensor biases (e.g. Holtappels et al. 2015, Reimers et al. 2016a), instrument orientation or tilt biases (e.g. Trowbridge 1998, Scully et al. 2016), or are actual transport at wave frequencies (Lumley and Terray 1983, Kuwae et al. 2006, Gerbi et al. 2008), the presented CPSD method, in combination with appropriate measurement heights, provides a specific framework to separate turbulent and wave-associated fluxes to overcome these biases, or to quantify fluxes associated with wave frequencies.

4.3 Sensors and Waves – The spectra for O_2 and H^+ do not show variability associated with the wave peaks present in the vertical and horizontal spectra, even during extreme wave conditions at the reef site. This suggests that the microfluidic sensor housing effectively removed wave bias from the sensors (Long and Nicholson 2018). The active pumping past the sensors created a constant-flow environment negating zero-crossing velocities and removed any concerns related to boundary layer, wave and pressure fluctuations and associated sensor response times (see Reimers et al. 2016a). These optical O_2 and H^+ ion selective field effect transistors (ISFET) sensors are sensitive to light interferance (Long et al. 2015a) and therefore benefited from the darkened housing, although light interferance for the O_2 optode only occurs in very shallow water due to its use of red light that is quickly attenuated with water depth. The rotating base allowed the precise correction for the separation between the sensors (Donis et al. 2015, Holtappels et al. 2015, Reimers et al. 2016a) using the known sensor separation, flow rate and the fact that that sensors were always oriented in line with the flow (Long et al. 2019). The Inertial Measurement Unit (IMU, housing a triaxial accelerometer, gyroscope, and magnetometer) measured the exact instrument orientation, movement and acceleration to allow for coordinate matrix transformation to account for platform rotation and movement (Long and Nicholson 2018). This new instrument design and motion correction is based on similar advancements used in atmospheric ship-based eddy covariance measurements to correct for ship motion (e.g., Edson et al. 1998, McGillis et al. 2001, Flügge et al. 2016).

This ECHOES measurement system including microfluidics (Long et al. 2015a) and IMU integration (Long and Nicholson 2018) represents a significant advancement of the EC technique that allow it to overcome previous challenges related to sensor wave bias and sensor separation corrections (Donis et al. 2015, Holtappels et al. 2015, Berg et al. 2015, Reimers et al. 2016b). However, while this ECHOES instrument design removed concerns related to sensor wave bias, it also complicated instrument engineering, had additional power requirements due to the use of a pump, and may not effectively rotate at very low current velocities. Importantly, this instrument configuration cannot remove bias in the vertical velocities used to calculate the flux. Thus, the presented combination of methodological improvements and the CPSD analysis framework is preferable to effectively remove wave bias from EC flux measurements. However, future studies applying O_2 optodes, O_2 Clark-type microsensors, or other sensors in a traditional, fixed, open-sensor EC instrument (e.g. Berg et al. 2003) will still benefit substantially from the CPSD analysis framework by removing wave bias caused by sensor sensitivity to wave velocities as well as removing wave frequencies that can cause bias in sensor separations corrections.

This manuscript presents the first use of a Honeywell Durafet® III pH sensor in an EC instrument. The reduction of noise in the signal was a major intial challenge with good results produced by using an optically coupled power supply and amplifier. However, it was still apparent that there was low density in the power spectra across frequencies, especially at the sand site. This is exhibited in the fairly flat power spectal density and low variance for the sand site (Figure 5d, 6d) and may idicate a lower threshold for resolving the H^+ flux (sand site, ± 0.03 µmol m^{-2} h^{-1}) whereas fluxes were about an order of magnitude larger at the seagrass and reef sites. This lower resolution for the H^+ data was also apparent in the highest error and lowest coefficients of determination when comparing the full-spectrum CPSD and EC flux caclulation methods. However, the use of H^+ ISFET sensors (along with O_2 sensors) is promising as a biogeochemical tracer due to its ability to be used in carbonate chemistry models to determine rates of calcification and dissolution (Long et al. 2015a, Takeshita et al. 2016).

4.4 Ecosystem Fluxes - The determined fluxes across the sites showed expected diel trends with generally positive O_2 fluxes during the daytime and negative O_2 fluxes at night. The H^+ fluxes showed the opposite diel trend, consistent with CO_2 consumption by photosynthesis during the day and CO_2 production by respiration at night. Both seagrass and sand O_2 fluxes exhibited net autotrophy, but the reef site showed strong heterotrophy likely due to the predominance of octocorals, algae, and rubble at this heavily degraded reef site (Hopkinson et al. 2020, Owens et al. 2020). Both the seagrass and sand O_2 fluxes are consistent with previous measurements nearby in a similar depth seagrass meadow by Long et al. (2015b) (NEM = 37 ± 31 mmol O_2 m^{-2} d^{-1}) and in a slightly deeper sandy site by Berg et al. (2016) (flux range = -2 to 4 mmol O_2 m^{-2} h^{-1}). The study sites were visited frequently during the afternoon and the production of bubbles was not observed at these sites, but we cannot conclusively determine that bubble ebullition of O_2 did not bias the presented O_2 fluxes (see Long et al. 2020). Notably, the reef net heterotrophy found here is a shift from the net autotrophy or balanced metabolism found nearby at Grecian Rocks Reef in 2009-2010 (Long et al. 2013) and may reflect differences between sites, the continuing degradation of the northern Florida Keys Reef tract (Muehllehner et al. 2016), and particularly to the proliferation of a bloom of red algae (*Galaxaura* spp.) following Hurricane Irma in 2017 that persisted through the time of our measurements in 2018 (Hopkinson et al. 2020, Owens et al. 2020). The H^+ fluxes observed at our sand site (± 0.03 µmol m^{-2} h^{-1}) are about an order of magnitude lower that those found at other biogenic calcium carbonate sandy sites (± 0.4 µmol m^{-2} h^{-1}, Cyronak et al. 2013) but these previous data were obtained in an isolated lagoon with large diel pH changes from about 7.8-8.4 that drove changes in dissolution and calcification (Santos et al. 2011, Cyronak et al. 2013) compared to the much lower diel pH (8.06 to 8.17) at our sand site. The large H^+ fluxes found at this isolated lagoon (± 0.4 µmol m^{-2} h^{-1}, Cyronak et al. 2013; -1.1 to 0.3 µmol m^{-2} h^{-1}, Santos et al. 2011) are more consistent with the magnitude of fluxes that were observed at our reef site (-0.5 to 1.1 µmol m^{-2} h^{-1}). The seagrass site was the only site that acted as a net acidity sink, consistent with studies that indicate seagrass meadows act as a carbon sink (e.g. Duarte et al. 2010).

4.5 Guidelines for Measurement Height and Sensor Response Time – In this study, the ADV and sensor measurement height above the sediment surface was determined by placing it at a height that was greater than twice the biological canopy or bedform height (Figure 1, Attard et al. 2014, Long et al. 2015c) as recommended by terrestrial EC guidelines where twice the canopy height, and up to 5 times the canopy height in patchy environments, is recommended (Burba and Anderson 2010). The resulting values for Eq. 3 ranged from 3.1 to 7.3 based on the site conditions, and it was evident that being substantially above the relationship suggested by Eq. 3 (e.g. Eq. 3 > 1, Scully et al. 2016) is beneficial to highlight and resolve the stable maxima produced prior to the wave frequencies (Figure 5, 6; Long et al. 2015c). Further, it is apparent that some studies sampled too close to the bottom to allow for spectral turbulence and wave separation as the mean of studies sampling < 0.25 m from the boundary fall directly on the surface defined by Eq. 3 = 1 (Figure 8a). Biological canopy heights (e.g. reef structures, macrophyte canopies) and physical roughness elements (e.g. grain size, bedforms) should also be considered when choosing measurement heights, as measurement heights are commonly reported from the benthic surface, not the surface of biological canopies that, in some cases, also vary in height with current velocity when the canopy is flexible (i.e. seagrasses, Nepf 2012).

With the recommended measurement heights, based on current velocities and wave period, it follows that if the reponse time of the sensor (typically represented as to the time to reach 90% of the total signal change) is twice as large as the determined cutoff frequency (i.e. the Nyquist frequency of F_c), the majority of the turbulent flux can be captured. Rearranging the equation $(2\pi z)/(UT_d)$ =3.1 (or the conservative minimum value demonstrated in this study to allow for separation of turbulence and wave frequencies) to solve for T_d and color shading by the assumption that the minimum response time is approximately the T_d (or the Nyquist frequency (2x) of the cutoff frequency [$F_c \approx 1/2T_d$]), produces a recommended minimum response time (t_{90}) based on site conditions (Figure 8b). For example, at a common shallow-water site where current velocity is ≤ 0.2 m s^{-1}, T_d is ≤ 4 s, and measurements are conducted 0.5 m from the top of the bottom roughness elements, a sensor with a t_{90} of ~ 5 s (0.2 Hz) can record all of the contributions to the CPSD flux acculumated up to the F_c. However, if the frequencies above the F_c are of interest due to potential advection of tubulence or porewater at wave frequencies (e.g. Lumley and Terray 1983, Kuwae et al. 2006, Gerbi et al. 2008), then a sensor that has a response time equivalent to the 2x the wave frequencies would be required. This role of physical transport at wave frequencies remains unresolved and requires further study, but is largely outside the main objectives of biogeochemical EC studies where chemical and turbulence sensor wave-bias is a major impediment.

There are additional factors to consider with sampling higher above the bottom including; increased bias in the fluxes due to storage within the water column, larger areas of integratation, or footprints, with increased measurement heights (Berg et al., 2003, Attard et al. 2014), increased time-lag for changes at the benthic surface to reach the measurement point (Rheuban and Berg 2013), and interaction with shear layers or strong concentration gradients during non-steady state conditions (Holtappels et al. 2013). These factors should be considered when choosing measurement heights, but can be minimized by sampling over long periods, and are generally small compared to the potential for wave-bias at shallow sites. For example, changes in storage in the water column are now commonly included with large measurement heights (Long et al. 2013, Rheuban et al. 2014a, Berger et al. 2020, Koopmans et al, 2020). Larger footprints are generally considered benefitial as they integrate benthic heterogeneity (Rheuban and Berg 2013). The time-lag between when the flux is released at the benthic surface and when it is recorded at the measurement height can be corrected when correlating fluxes to environmental driving variables (i.e. irradiance, tides, concentrations) (Rheuban and Berg 2013). Further, the effects of all potential biases can be reduced by increasing deployment duration, especially over a variety of non-steady state conditions to better integrate flux estimates through time (Holtappels et al. 2013). Therefore, considering the substantial benefit of sampling higher above the bottom to remove wave bias, and the lower risk of other factors above, it is recommended to use adequate measurement heights (e.g. Figure 8b) at shallow sites where waves may be present.

4.6 Application to Similar Flux Techniques - The gradient flux, or profile flux, technique relies on the same boundary layer assumptions as the EC technique, but uses measurements of the gradients or profile of current velocity and solute concentrations through the boundary layer (McGillis et al. 2009, McGillis et al. 2011, Turk et al. 2015, Takeshita et al. 2016). Similar to the development of aquatic EC, the scalar transport of gas and water fluxes in the marine atmospheric boundary layer steered these developments (McGillis et al. 2001, Zappa et al. 2003, Edson et al. 2004). In the gradient flux technique, the flux of a solute is calculated as:

$$Flux = -K_z \frac{\partial C}{\partial z} \qquad \textit{Eq. 4.}$$

where $-K_z$ is the eddy diffusivity, and $\frac{\partial C}{\partial z}$ is the benthic concentration gradient usually measured using a pair of chemical sensors or a dual-height pumping system at known heights (z) above the bottom (Takeshita et al. 2016). Gradient exchange fluxes are determined by taking the integral of Eq.4 across ∂z and using the relationship $K_z = u^*\kappa z$ (where u^* is the friction velocity and κ is Von Karman's constant) (McGillis et al. 2009). The resulting relationship $[Flux = u^*\kappa((C_{z_2} - C_{z_1})/\log(z_2/z_1))]$ determines u^* from logarithmic fits to benthic current profiles, which is an assumption that is often problematic in high roughness shallow systems during low flow conditions in the presence of waves (Holtappels and Lorke 2011, Nepf 2012, Trowbridge and Lentz 2018). The gradient exchange technique has been primarily applied in shallow coastal seagrass and reef ecosystems (McGillis et al. 2009, Turk et al. 2015, Takeshita et al. 2016) and could benefit from the new analysis framework applied here by the direct calculation of K_z. Assuming a Prandtl number of 1, the eddy diffusivity can be calculated by:

$$K_z = (\overline{u'w'})/\frac{\partial U}{\partial z} \qquad \textit{Eq. 5.}$$

where $(\overline{u'w'})$ is the momentum flux (e.g. Eq. 1) and $\frac{\partial U}{\partial z}$ is the shear calculated from a velocity profile of mean flow (Holtappels and Lorke 2011). Using the CPSD accumulation for determining the momentum fluxes will yield direct measurements of K_z, which is superior to the assumption of a logarithmic boundary layer current profile, especially in high-roughness shallow environments (Holtappels and Lorke 2011) such as coral reefs and seagrass beds where flow profiles often do not follow a logarithmic relationship (Nepf 2012). For example, the momentum fluxes calculated from traditional covariance analysis produced substantially larger values (Table 2, Figure 4) and accumulating the CPSD below the wave frequencies will enable a more accurate determination of K_z for the gradient exchange technique while removing the need to assume a logarithmic boundary layer current profile.

5 Summary

The review of aquatic biogeochemical EC literature has revealed that biases created by waves have complicated the use of aquatic EC in shallow waters at a time when coastal processes are gaining recognition as important factors in nearshore water quality, regional biogeochemical cycles and global modeling efforts. However, the conditions and instrument configurations used during previous studies suggest that a fundamental shift in how EC measurements are conducted and analyzed can overcome these limitations. The new analysis framework presented here, including using appropriate measurement heights and CPSD accumulation up to wave frequencies, demonstrates and that full-spectrum CPSD analysis in consistent with traditional EC analysis, and that wave-bias apparent in traditional EC analysis can be removed through exclusion of waves frequencies using spectral CPSD accumulation. By using the new approaches presented here (spectral filtering, microfluidics, rotating instrument) turbulent fluxes can be determined without contamination from current velocities, surface waves, or bias due to sensor separation. The spectral analysis framework can also be applied to standard eddy covariance and gradient exchange systems to reduce the bias created by wave-sensitive sensors and bias in turbulence and velocity measurements. The application of the presented spectral analysis framework requires measurements to be conducted at sufficient heights from the interface, and also has the significant benefit of allowing for chemical sensors with slower response times, enabling new sensor and tracer applications to the EC technique.

Acknowledgments

This work benefitted from numerous discussions with Malcolm Scully, John Trowbridge, Jennie Rheuban, Wade McGillis, and the wider aquatic EC community, in general. We thank Jennie Rheuban, Daniel McCorkle, Brian Hopkinson, and Kyle Conner for assistance with field work. This work was supported by the Independent Research & Development Program at WHOI and NSF OCE grants 1657727 and 1633951. The author declares no conflict of interest. Data for this study are archived at the Biological & Chemical Oceanography Data Management Office per NSF policies (https://www.bco-dmo.org/person/560155).

References Cited

Attard, K.M., Glud, R.N., McGinnis, D.F. and Rysgaard, S., 2014. Seasonal rates of benthic primary production in a Greenland fjord measured by aquatic eddy correlation. *Limnology and Oceanography*, *59*(5), pp.1555-1569. doi:10.4319/lo.2014.59.5.1555

Attard, K.M., Stahl, H., Kamenos, N.A., Turner, G., Burdett, H.L. and Glud, R.N., 2015. Benthic oxygen exchange in a live coralline algal bed and an adjacent sandy habitat: an eddy covariance study. *Marine Ecology Progress Series*, *535*, pp.99-115.

Attard, K.M., Hancke, K., Sejr, M.K. and Glud, R.N., 2016. Benthic primary production and mineralization in a High Arctic fjord: in situ assessments by aquatic eddy covariance. *Marine ecology progress series*, *554*, pp.35-50.

Attard, K.M., Søgaard, D.H., Piontek, J., Lange, B.A., Katlein, C., Sørensen, H.L., McGinnis, D.F., Rovelli, L., Rysgaard, S., Wenzhöfer, F. and Glud, R.N., 2018. Oxygen fluxes beneath Arctic land-fast ice and pack ice: towards estimates of ice productivity. *Polar Biology*, *41*(10), pp.2119-2134.

Attard, K.M., Rodil, I.F., Glud, R.N., Berg, P., Norkko, J. and Norkko, A., 2019. Seasonal ecosystem metabolism across shallow benthic habitats measured by aquatic eddy covariance. *Limnology and oceanography letters*, *4*(3), pp.79-86. doi: 10.1002/lol2.10107

Baldocchi DD (2003) Assessing the eddy covariance technique for evaluating carbon dioxide exchange rates of ecosystems: past, present and future. *Global Change Biology* **9**: 479-492. DOI: 10.1046/j.1365-2486.2003.00629.x

Berg, P., H. Røy, F. Janssen, V. Meyer, B. Jørgensen, M. Huettel, and D. de Beer (2003), Oxygen uptake by aquatic sediments measured with a novel non-invasive eddy-correlation technique, Mar. Ecol. Prog. Ser., 261, 75-83, doi:10.3354/meps261075.

Berg, P. and Huettel, M., 2008. Monitoring the seafloor using the noninvasive eddy correlation technique. *Oceanography*, *21*(4), pp.164-167.

Berg, P., Glud, R.N., Hume, A., Stahl, H., Oguri, K., Meyer, V. and Kitazato, H., 2009. Eddy correlation measurements of oxygen uptake in deep ocean sediments. *Limnology and Oceanography: Methods*, *7*(8), pp.576-584. doi.org/10.4319/lom.2009.7.576

Berg, P., Long, M.H., Huettel, M., Rheuban, J.E., McGlathery, K.J., Howarth, R.W., Foreman, K.H., Giblin, A.E. and Marino, R., 2013. Eddy correlation measurements of oxygen fluxes in permeable sediments exposed to varying current flow and light. *Limnology and Oceanography*, *58*(4), pp.1329-1343.

Berg, P., C. E. Reimers, J. Rosman, T. Özkan-Haller, M. Huettel, M. L. Delgard. (2015). Technical Note: Time lag correction of aquatic eddy covariance data measured in the presence of waves. Biogeosciences Discuss. 12: 8395-8427. doi: 10.5194/bgd-12-8395-2015.

Berg, P., Koopmans, D.J., Huettel, M., Li, H., Mori, K. and Wüest, A., 2016. A new robust oxygen-temperature sensor for aquatic eddy covariance measurements. *Limnology and Oceanography: Methods*, *14*(3), pp.151-167. doi.org/10.1002/lom3.10071

Berg, P. and Pace, M.L., 2017. Continuous measurement of air–water gas exchange by underwater eddy covariance. *Biogeosciences*, *14*(23), pp.5595-5606. doi.org/10.5194/bg-14-5595-2017

Berg, P., Delgard, M.L., Polsenaere, P., McGlathery, K.J., Doney, S.C. and Berger, A.C., 2019. Dynamics of benthic metabolism, O2, and pCO2 in a temperate seagrass meadow. *Limnology and Oceanography*, *64*(6), pp.2586-2604.

Berger, A.C., Berg, P., McGlathery, K.J. and Delgard, M.L., 2020. Long-term trends and resilience of seagrass metabolism: A decadal aquatic eddy covariance study. *Limnology and Oceanography*.

Brand, A, McGinnis, D.F., Wehrli, B., Wuest, A. 2008. Intermittent oxygen flux from the interior into the bottom boundary of lakes as observed by eddy correlation. *Limnology and Oceanography*, 53(5), pp. 1997-2006.

Burba, G. and Anderson, D., (2010). A brief practical guide to eddy covariance flux measurements: principles and workflow examples for scientific and industrial applications. LI-COR Biosciences, Lincoln, Nebraska, USA, 212 pp.: http://www.licor.com/eddycovariance

Cathalot, C., Oevelen, D.V., Cox, T.J., Kutti, T., Lavaleye, M.S., Duineveld, G.C., & Meysman, F.J. (2015). Cold-water coral reefs and adjacent sponge grounds: hotspots of benthic respiration and organic carbon cycling in the deep sea. *Frontiers in Marine Science, 2*, 1-12.

Chipman, L., Huettel, M., Berg, P., Meyer, V., Klimant, I., Glud, R. and Wenzhoefer, F., 2012. Oxygen optodes as fast sensors for eddy correlation measurements in aquatic systems. *Limnology and Oceanography: Methods*, *10*(5), pp.304-316.

Crusius, J., Berg, P., Koopmans, D.J. and Erban, L., 2008. Eddy correlation measurements of submarine groundwater discharge. *Marine Chemistry*, *109*(1-2), pp.77-85.

Cyronak, T., Santos, I.R., McMahon, A. and Eyre, B.D., 2013. Carbon cycling hysteresis in permeable carbonate sands over a diel cycle: Implications for ocean acidification. *Limnology and Oceanography*, *58*(1), pp.131-143. doi.org/10.4319/lo.2013.58.1.0131

de Froe, E., Rovelli, L., Glud, R.N., Maier, S.R., Duineveld, G., Mienis, F., Lavaleye, M. and van Oevelen, D., 2019. Benthic oxygen and nitrogen exchange on a cold-water coral reef in the North-East Atlantic Ocean. *Frontiers in Marine Science*, *6*, p.665.

Donis, D., Holtappels, M., Noss, C., Cathalot, C., Hancke, K., Polsenaere, P., & McGinnis, D. F. (2015). An assessment of the precision and confidence of aquatic eddy correlation measurements. *Journal of Atmospheric and Oceanic Technology*, *32*(3), 642-655. doi.org/10.1175/JTECH-D-14-00089.1

Donis, D., McGinnis, D.F., Holtappels, M., Felden, J. and Wenzhoefer, F., 2016. Assessing benthic oxygen fluxes in oligotrophic deep sea sediments (HAUSGARTEN observatory). *Deep Sea Research Part I: Oceanographic Research Papers*, *111*, pp.1-10.

Duarte, C.M., Marbà, N., Gacia, E., Fourqurean, J.W., Beggins, J., Barrón, C. and Apostolaki, E.T., 2010. Seagrass community metabolism: Assessing the carbon sink capacity of seagrass meadows. *Global Biogeochemical Cycles*, *24*(4). doi.org/10.1029/2010GB003793

Edson, J. B., Hinton, A. A., Prada, K. E., Hare, J. E., & Fairall, C. W. (1998). Direct covariance flux estimates from mobile platforms at sea. *Journal of Atmospheric and Oceanic Technology*, *15*(2), 547-562. doi.org/10.1175/1520-0426(1998)015<0547:DCFEFM>2.0.CO;2

Edson, J.B., Zappa, C.J., Ware, J.A., McGillis, W.R. and Hare, J.E., 2004. Scalar flux profile relationships over the open ocean. *Journal of Geophysical Research: Oceans*, *109*(C8). doi.org/10.1029/2003JC001960

Else, B.G.T., Rysgaard, S., Attard, K., Campbell, K., Crabeck, O., Galley, R.J., Geilfus, N.X., Lemes, M., Lueck, R., Papakyriakou, T. and Wang, F., 2015. Under-ice eddy covariance flux measurements of heat, salt, momentum, and dissolved oxygen in an artificial sea ice pool. *Cold Regions Science and Technology*, *119*, pp.158-169.

Fairaill, C.W., Hare, J.E., Edson, J.B. and McGillis, W., 2000. Parameterization and micrometeorological measurement of air–sea gas transfer. *Boundary-Layer Meteorology*, *96*(1-2), pp.63-106.

Flügge, M., Paskyabi, M. B., Reuder, J., Edson, J. B., & Plueddemann, A. J. (2016). Comparison of Direct Covariance Flux Measurements from an Offshore Tower and a Buoy. *Journal of Atmospheric and Oceanic Technology*, *33*(5), 873-890. doi.org/10.1175/JTECH-D-15-0109.1

Gerbi, G.P., Trowbridge, J.H., Edson, J.B., Plueddemann, A.J., Terray, E.A. and Fredericks, J.J. 2008. Measurements of momentum and heat transfer across the air–sea interface. Journal of Physical Oceanography, 38(5), 1054-1072. doi.org/10.1175/2007JPO3739.1

Glud, R.N., Berg, P., Hume, A., Batty, P., Blicher, M.E., Lennert, K. and Rysgaard, S., 2010. Benthic O2 exchange across hard-bottom substrates quantified by eddy correlation in a sub-Arctic fjord. *Marine ecology progress series*, *417*, pp.1-12.

Glud, R.N., Rysgaard, S., Turner, G., McGinnis, D.F. and Leakey, R.J., 2014. Biological-and physical-induced oxygen dynamics in melting sea ice of the Fram Strait. *Limnology and oceanography*, *59*(4), pp.1097-1111.

Glud, R.N., Berg, P., Stahl, H., Hume, A., Larsen, M., Eyre, B.D. and Cook, P.L., 2016. Benthic carbon mineralization and nutrient turnover in a Scottish sea loch: an integrative in situ study. *Aquatic Geochemistry*, *22*(5-6), pp.443-467.

Holtappels, M. and Lorke, A., 2011. Estimating turbulent diffusion in a benthic boundary layer. *Limnology and Oceanography: Methods*, *9*(1), pp.29-41.

Holtappels, M., Glud, R.N., Donis, D., Liu, B., Hume, A., Wenzhöfer, F. and Kuypers, M.M., 2013. Effects of transient bottom water currents and oxygen concentrations on benthic exchange rates as assessed by eddy correlation measurements. *Journal of Geophysical Research: Oceans*, *118*(3), pp.1157-1169. doi.org/10.1002/jgrc.20112

Holtappels, M., Noss, C., Hancke, K., Cathalot, C., McGinnis, D. F., Lorke, A., & Glud, R. N. (2015). Aquatic Eddy Correlation: Quantifying the Artificial Flux Caused by Stirring-Sensitive O_2 Sensors. PloS one, 10(1), e0116564. doi.org/10.1371/journal.pone.0116564

Hopkinson BM, King AC, Johnson-Roberson M, Long MH, Bhandarkar M. (2020) Automated classification of three-dimensional reconstructions of coral reefs using convolutional neural networks. PLoS ONE 15(3): e0230671. DOI: 10.1371/journal.pone.0230671

Hume, A, P Berg, KJ McGlathery. (2011) Dissolved oxygen fluxes and ecosystem metabolism in an eelgrass (*Zostera marina*) meadow measured with the novel eddy correlation technique. *Limnol. Oceanogr*. **56**: 86–96.

Johnson, K.S., Barry, J.P., Coletti, L.J., Fitzwater, S.E., Jannasch, H.W. and Lovera, C.F., 2011. Nitrate and oxygen flux across the sediment-water interface observed by eddy correlation measurements on the open continental shelf. *Limnology and Oceanography: Methods*, *9*(11), pp.543-553.

Klimant, I., Meyer, V. and Kühl, M., 1995. Fiber-optic oxygen microsensors, a new tool in aquatic biology. *Limnology and Oceanography*, *40*(6), pp.1159-1165.

Koopmans, D.J. and Berg, P., 2015. Stream oxygen flux and metabolism determined with the open water and aquatic eddy covariance techniques. *Limnology and Oceanography*, *60*(4), pp.1344-1355.

Koopmans, D., Holtappels, M., Chennu, A., Weber, M. and de Beer, D., 2020. High Net Primary Production of Mediterranean Seagrass (Posidonia oceanica) Meadows Determined With Aquatic Eddy Covariance. *Frontiers in marine science*, *7*: 118. doi: 10.3389/fmars.2020.00118

Kreling, J., Bravidor, J., McGinnis, D.F., Koschorreck, M. and Lorke, A., 2014. Physical controls of oxygen fluxes at pelagic and benthic oxyclines in a lake. *Limnology and Oceanography*, *59*(5), pp.1637-1650. doi.org/10.4319/lo.2014.59.5.1637

Kuwae, T., Kamio, K., Inoue, T., Miyoshi, E. and Uchiyama, Y., 2006. Oxygen exchange flux between sediment and water in an intertidal sandflat, measured in situ by the eddy-correlation method. *Marine Ecology Progress Series*, *307*, pp.59-68.

Lee, J.S., Kang, D.J., Hineva, E., Slabakova, V., Todorova, V., Park, J. and Cho, J.H., 2017. Estimation of net ecosystem metabolism of seagrass meadows in the coastal waters of the East Sea and Black Sea using the noninvasive eddy covariance technique. *Ocean Science Journal*, *52*(2), pp.243-256.

Lee, X., W. Massman, and B. Law (Eds.).2004. "Handbook of Micrometeorology: A Guide for Surface Flux Measurement and Analysis". Springer-Verlag, 250 pp.

Long, M.H., Rheuban, J.E., Berg, P. and Zieman, J.C., 2012b. A comparison and correction of light intensity loggers to photosynthetically active radiation sensors. *Limnology and Oceanography: Methods*, *10*(6), pp.416-424.

Long, M.H., Koopmans, D., Berg, P., Rysgaard, S., Glud, R.N. and Søgaard, D.H., 2012a. Oxygen exchange and ice melt measured at the ice-water interface by eddy correlation. *Biogeosciences*, *9*(6). doi:10.5194/bg-9-1957-2012

Long, M. H., P. Berg, D. de Beer, and J. C. Zieman (2013), In situ coral reef oxygen metabolism: an eddy correlation study., PLoS One, 8(3), e58581, doi:10.1371/journal.pone.0058581.

Long, M.H., Charette, M.A., Martin, W.R. and McCorkle, D.C., 2015a. Oxygen metabolism and pH in coastal ecosystems: Eddy Covariance Hydrogen ion and Oxygen Exchange System (ECHOES). *Limnology and Oceanography: Methods*, *13*(8), pp.438-450. doi:10.1002/lom3.10038.

Long, M. H., P. Berg, K. J. McGlathery, and J. C. Zieman (2015b), Sub-tropical seagrass ecosystem metabolism measured by eddy covariance, Mar. Ecol. Prog. Ser., 529, 75–90, doi:10.3354/meps11314.

Long, M.H., Berg, P. and Falter, J.L., 2015c. Seagrass metabolism across a productivity gradient using the eddy covariance, Eulerian control volume, and biomass addition techniques. *Journal of Geophysical Research: Oceans*, *120*(5), pp.3624-3639. doi.org/10.1002/2014JC010352

Long, M.H. and Nicholson, D.P., 2018. Surface gas exchange determined from an aquatic eddy covariance floating platform. *Limnology and Oceanography: Methods*, *16*(3), pp.145-159. doi.org/10.1002/lom3.10233

Long, M.H., Rheuban, J.E., McCorkle, D.C., Burdige, D.J. and Zimmerman, R.C., 2019. Closing the oxygen mass balance in shallow coastal ecosystems. *Limnology and Oceanography*, *64*(6), pp.2694-2708. doi.org/10.1002/lno.11248

Long, M.H., Sutherland, K., Wankel, S.D., Burdige, D.J. and Zimmerman, R.C., 2020. Ebullition of oxygen from seagrasses under supersaturated conditions. *Limnology and oceanography*, *65*(2), pp.314-324. doi.org/10.1002/lno.11299

Lorke, A., McGinnis, D.F., Maeck, A. and Fischer, H., 2012. Effect of ship locking on sediment oxygen uptake in impounded rivers. *Water Resources Research*, *48*(12).

Lorke, A., McGinnis, D.F. and Maeck, A., 2013. Eddy-correlation measurements of benthic fluxes under complex flow conditions: Effects of coordinate transformations and averaging time scales. Limnology and Oceanography: Methods, 11(8), pp.425-437.

Lorrai, C., McGinnis, D.F., Berg, P., Brand, A. and Wüest, A., 2010. Application of oxygen eddy correlation in aquatic systems. *Journal of Atmospheric and Oceanic Technology*, *27*(9), pp.1533-1546.

Lumley, J.L. and Terray, E.A., 1983. Kinematics of turbulence convected by a random wave field. Journal of Physical Oceanography, 13(11), pp.2000-2007.

McCann-Grosvenor, K., Reimers, C.E. and Sanders, R.D., 2014. Dynamics of the benthic boundary layer and seafloor contributions to oxygen depletion on the Oregon inner shelf. *Continental Shelf Research*, *84*, pp.93-106.

McGillis, W.R., Edson, J.B., Hare, J.E. and Fairall, C.W., 2001. Direct covariance air-sea CO_2 fluxes. *Journal of Geophysical Research: Oceans*, *106*(C8), pp.16729-16745. doi.org/10.1029/2000JC000506

McGillis, W. R., C. Langdon, A. J. Williams, B. Loose, 2009. O_2 MAVS: an Instrument for Measuring Oxygen Flux, MTS/IEEE Biloxi - Marine Technology for Our Future: Global and Local Challenges, OCEANS 2009, No. 5422166**.**

McGillis, W. R., C. Langdon, B. Loose, K. K.Yates, J. Corredor, 2011. Productivity of a coral reef using boundary layer and enclosure methods, *Geophys. Res. Lett.*, 38, L L03611, doi:10.1029/2010GL046179.

McGinnis, D.F., Berg, P., Brand, A., Lorrai, C., Edmonds, T.J. and Wüest, A., 2008. Measurements of eddy correlation oxygen fluxes in shallow freshwaters: Towards routine applications and analysis. *Geophysical Research Letters*, *35*(4).

McGinnis, D.F., Cherednichenko, S., Sommer, S., Berg, P., Rovelli, L., Schwarz, R., Glud, R.N. and Linke, P., 2011. Simple, robust eddy correlation amplifier for aquatic dissolved oxygen and hydrogen sulfide flux measurements. *Limnology and Oceanography: Methods*, *9*(8), pp.340-347.

McGinnis, D.F., Sommer, S., Lorke, A., Glud, R.N. and Linke, P., 2014. Quantifying tidally driven benthic oxygen exchange across permeable sediments: An aquatic eddy correlation study. *Journal of Geophysical Research: Oceans*, *119*(10), pp.6918-6932.

Muehllehner, N., Langdon, C., Venti, A. and Kadko, D., 2016. Dynamics of carbonate chemistry, production, and calcification of the Florida Reef Tract (2009–2010): Evidence for seasonal dissolution. *Global Biogeochemical Cycles*, *30*(5), pp.661-688. doi.org/10.1002/2015GB005327

Murniati, E., Geissler, S. and Lorke, A., 2015. Short-term and seasonal variability of oxygen fluxes at the sediment–water interface in a riverine lake. *Aquatic Sciences*, *77*(2), pp.183-196.

Nepf, H.M., 2012. Flow and transport in regions with aquatic vegetation. *Annu. Rev. Fluid Mech. 2012. 44:123–42*. doi: 10.1146/annurev-fluid-120710-101048

Owen DP, Long MH, Fitt WK, Hopkinson BM. Taxon-specific primary production rates on coral reefs in the Florida Keys. Limnology and Oceanography. LO-20-0165

Plew, D.R., 2019. Investigating benthic impacts at salmon farms using eddy covariance measurements of benthic oxygen fluxes. *Aquaculture Environment Interactions*, *11*, pp.337-357.

Reidenbach, M.A., Berg, P., Hume, A., Hansen, J.C. and Whitman, E.R., 2013. Hydrodynamics of intertidal oyster reefs: The influence of boundary layer flow processes on sediment and oxygen exchange. *Limnology and Oceanography: Fluids and Environments*, *3*(1), pp.225-239.

Reimers, C.E., Özkan-Haller, H., Berg, P., Devol, A., McCann-Grosvenor, K. and Sanders, R.D., 2012. Benthic oxygen consumption rates during hypoxic conditions on the Oregon continental shelf: Evaluation of the eddy correlation method. *Journal of Geophysical Research: Oceans*, *117*(C2).

Reimers, C. E., Özkan-Haller, H. T., Albright, A. T., & Berg, P. (2016a). Microelectrode velocity effects and aquatic eddy covariance measurements under waves. *Journal of Atmospheric and Oceanic Technology*, *33*(2), 263-282.

Reimers, C.E., Özkan-Haller, H.T., Sanders, R.D., McCann-Grosvenor, K., Chace, P.J. and Crowe, S.A., 2016b. The dynamics of benthic respiration at a mid-shelf station off Oregon. *Aquatic geochemistry*, *22*(5-6), pp.505-527.

Revsbech, N.P., 1989. An oxygen microsensor with a guard cathode. *Limnology and Oceanography*, *34*(2), pp.474-478.

Rheuban JE and P Berg (2013) The effects of spatial and temporal variability at the sediment surface on aquatic eddy correlation flux measurements. *Limnol Oceanogr Meth* **11**: 351-359.

Rheuban, J.E., Berg, P. and McGlathery, K.J., 2014a. Multiple timescale processes drive ecosystem metabolism in eelgrass (Zostera marina) meadows. *Marine Ecology Progress Series*, *507*, pp.1-13.

Rheuban, J.E., Berg, P. and McGlathery, K.J., 2014b. Ecosystem metabolism along a colonization gradient of eelgrass (Zostera marina) measured by eddy correlation. *Limnology and oceanography*, *59*(4), pp.1376-1387.

Rodil, I.F., Attard, K.M., Norkko, J., Glud, R.N. and Norkko, A., 2019. Towards a sampling design for characterizing habitat-specific benthic biodiversity related to oxygen flux dynamics using Aquatic Eddy Covariance. *PloS one*, *14*(2).

Rovelli, L., Attard, K.M., Bryant, L.D., Flögel, S., Stahl, H., Roberts, J.M., Linke, P. and Glud, R.N., 2015. Benthic O2 uptake of two cold-water coral communities estimated with the non-invasive eddy correlation technique. *Marine Ecology Progress Series*, *525*, pp.97-104.

Rovelli, L., Attard, K.M., Binley, A., Heppell, C.M., Stahl, H., Trimmer, M. and Glud, R.N., 2017. Reach-scale river metabolism across contrasting sub-catchment geologies: Effect of light and hydrology. *Limnology and oceanography*, *62*(S1), pp.S381-S399.

Rovelli, L., Attard, K.M., Heppell, C.M., Binley, A., Trimmer, M. and Glud, R.N., 2018. Headwater gas exchange quantified from O_2 mass balances at the reach scale. *Limnology and Oceanography: Methods*, *16*(10), pp.696-709.

Rovelli, L., Attard, K.M., Cárdenas, C.A. and Glud, R.N., 2019. Benthic primary production and respiration of shallow rocky habitats: a case study from South Bay (Doumer Island, Western Antarctic Peninsula). *Polar biology*, *42*(8), pp.1459-1474.

Santos, I.R., Glud, R.N., Maher, D., Erler, D. and Eyre, B.D., 2011. Diel coral reef acidification driven by porewater advection in permeable carbonate sands, Heron Island, Great Barrier Reef. *Geophysical Research Letters*, *38*(3). doi:10.1029/2010GL046053

Scully, M.E., Trowbridge, J.H. and Fisher, A.W., 2016. Observations of the transfer of energy and momentum to the oceanic surface boundary layer beneath breaking waves. *Journal of Physical Oceanography*, *46*(6), pp.1823-1837. doi.org/10.1175/JPO-D-15-0165.1

Shaw, W.J. and Trowbridge, J.H., 2001. The direct estimation of near-bottom turbulent fluxes in the presence of energetic wave motions. *Journal of Atmospheric and Oceanic Technology*, *18*(9), pp.1540-1557.

Swinbank, W.C., 1951. The measurement of vertical transfer of heat and water vapor by eddies in the lower atmosphere. *Journal of Meteorology*, *8*(3), pp.135-145.

Takeshita, Y., W.R. McGillis, E.M. Briggs, A.L. Carter, E.M. Donham, T.R. Martz (2016). Assessment of net community production and calcification of a coral reef using a boundary layer approach. *Journal of Geophysical Research: Oceans,* 121 (8), 5655-5671.

Trowbridge, J.H., 1998. On a technique for measurement of turbulent shear stress in the presence of surface waves. *Journal of Atmospheric and Oceanic Technology*, *15*(1), pp.290-298.

Trowbridge, J.H. and Lentz, S.J., 2018. The bottom boundary layer. *Annual review of marine science*, *10*, pp.397-420.

Trowbridge, J., Scully, M. and Sherwood, C.R., 2018. The cospectrum of stress-carrying turbulence in the presence of surface gravity waves. *Journal of Physical Oceanography*, *48*(1), pp.29-44. doi.org/10.1175/JPO-D-17-0016.1

Turk, D., J.M. Bedard, W.J. Burt, S. Vagle, H. Thomas, K. Azetsu-Scott, W. R. McGillis (2016) Inorganic carbon in a high latitude estuary-fjord system in Canada's eastern Arctic. *Estuarine, Coastal and Shelf Science,* 178, 137-147.

Volaric, M.P., Berg, P. and Reidenbach, M.A., 2018. Oxygen metabolism of intertidal oyster reefs measured by aquatic eddy covariance. *Marine Ecology Progress Series*, *599*, pp.75-91.

Volaric, M.P., Berg, P. and Reidenbach, M.A., 2019. An invasive macroalga alters ecosystem metabolism and hydrodynamics on a tidal flat. *Marine Ecology Progress Series*, *628*, pp.1-16.

Volaric, M.P., Berg, P. and Reidenbach, M.A., 2020. Drivers of Oyster Reef Ecosystem Metabolism Measured Across Multiple Timescales. *Estuaries and Coasts*, pp.1-12.

Weck, J. and Lorke, A., 2017. Mixing efficiency in the thermocline of lakes observed from eddy correlation flux measurements. *Journal of Geophysical Research: Oceans*, *122*(1), pp.291-305. doi.org/10.1002/2016JC012188

Wyngaard, J.C. and Coté, O.R., 1972. Cospectral similarity in the atmospheric surface layer. *Quarterly Journal of the Royal Meteorological Society*, *98*(417), pp.590-603.

Yamamoto, S., Kayanne, H., Tokoro, T., Kuwae, T. and Watanabe, A., 2015. Total alkalinity flux in coral reefs estimated from eddy covariance and sediment pore-water profiles. *Limnology and Oceanography*, *60*(1), pp.229-241.

Zappa, C. J., P. A. Raymond, E. A. Terray, and W. R. McGillis, 2003. Variation in surface turbulence and the gas transfer velocity over a tidal cycle in a macro-tidal estuary, *Estuaries*, Vol. 26, No. 6, 1401-1415.

AGU PUBLICATIONS

Journal of Geophysical Research: Oceans

Supporting Information for

Aquatic Biogeochemical Eddy Covariance Fluxes in the Presence of Waves

Matthew H. Long[1]

[1]Marine Chemistry and Geochemistry Department, Woods Hole Oceanographic Institution, 266 Woods Hole Road, MS#8, Woods Hole, Massachusetts, USA, 02543

Contents of this file

Additional Supporting Information (Files uploaded separately)

Table S1

Text S1.

The attached Supplementary Table 1 (Characteristics of Field Studies using Eddy Covariance) shows all aquatic EC field studies that were reviewed for this study, with summary data shown in Figure 2. An example of response time tests for the Honeywell Durafet III pH sensor is shown in supplementary Figure S1, which was conducted by pumping pH buffer solutions through the microfluidic housing (Figure S2), with switching conducted manually using a valve. The construction and application of the microfluidic housing is shown in Figure S2. The difference between standard EC fluxes and those calculated by the accumulated CPSD (< 0.125 Hz) analyses are shown in Figure S3, where the residual differences are plotted versus the wave velocity.

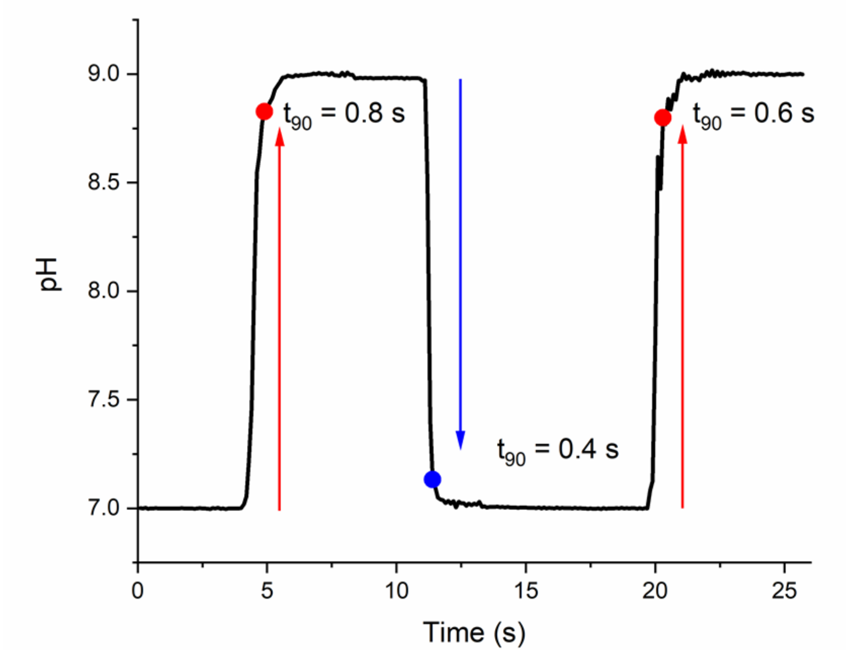

Figure S1. Example of repeated response time tests of a Honeywell Durafet pH sensor utilizing the microfluidic chamber (Figure S2), two pH buffers (7.0 and 9.0), a KNF10 micropump (100mL min^{-1}) and a simple Leur Lock valve to switch between the solutions. The 90% response time (t_{90}) is reported as the time needed to reach 90% of the total signal change (dots).

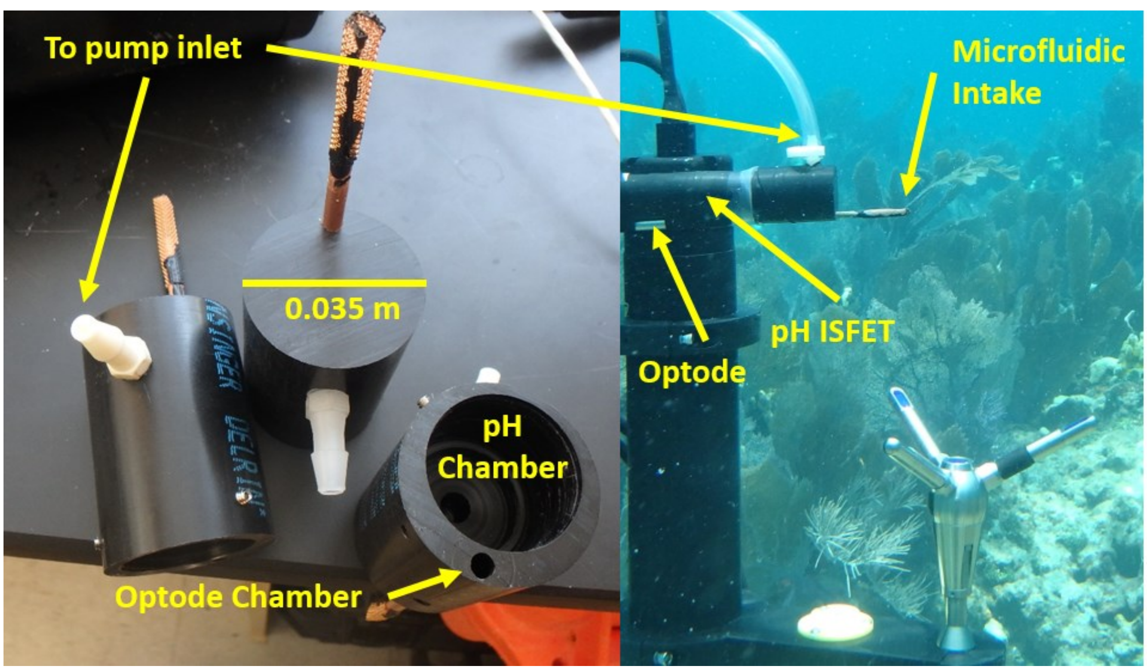

Figure S2. Construction (left) and application at the reef site (right) of the microfluidic chambers that houses the O2 optode and Honeywell Durafet sensors.

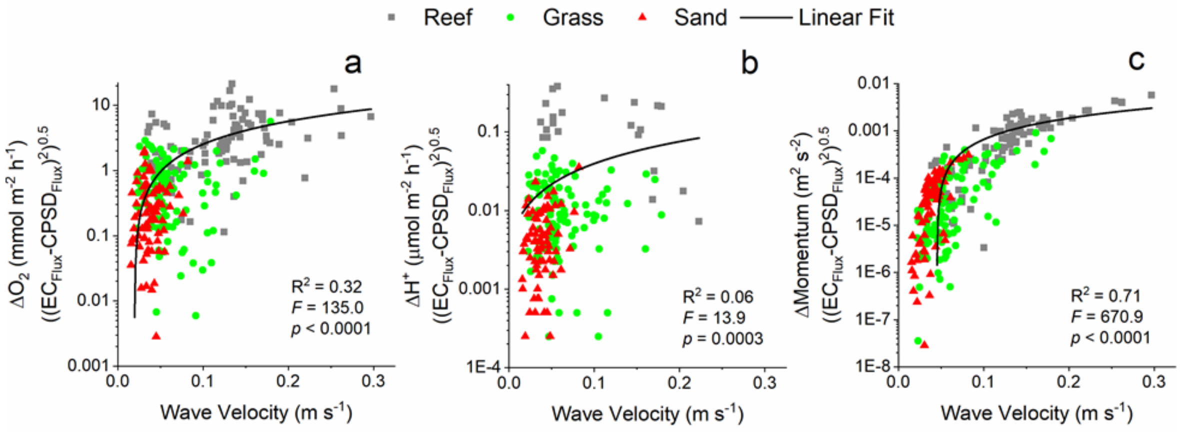

Figure S3. Absolute difference between the hourly eddy covariance and CPSD (< 0.125 Hz) fluxes compared to wave velocities. Linear fits are performed across all 3 sites. Statistics represent a difference compared to a zero-slope line.

Table S1. Field-based, biogeochemical, aquatic eddy covariance studies and the parameters and conditions of previous studies.